Liquid Crystals
Vol. 00, No. 00, Month 200x, 1–26

Articles

Twist-bend nematic phases in binary mixtures of banana-shaped liquid crystalline molecules

Akihiko Matsuyama*

Department of Bioscience and Bioinformatics, Faculty of Computer Science and Systems Engineering, Kyushu Institute of Technology, Kawazu 680-4, Iizuka, Fukuoka 820-8502, JAPAN

(*May. 2017*)

We present a mean field theory to describe twist-bend nematic (N_{TB}) phases in binary mixtures of banana-shaped, such as bent-core or dimer, liquid crystalline (LC) molecules with $K_{22} > K_{33}$, where K_{22} is a twist and K_{33} is a bend elastic constant. We introduce the free energy for the mixtures by taking into account the director-pitch (DP) coupling γ_i of the consisting LC molecules $i(= A, B)$ and calculate the phase diagrams on the temperature-concentration plane. Our theory demonstrates that the isotropic (I), or para-nematic (pN), nematic (N), and N_{TB} phases appear, depending on the strength of the DP coupling parameter γ_i and predicts various phase transitions: the first-order $N - pN(I)$ and $N_{TB} - pN(I)$ transitions, and the second-order $N_{TB} - N$ transition, etc, on the temperature-concentration plane. Our theory has a good agreement with the experimental phase diagrams of the mixtures.

Keywords: twist-bend nematic; cholesteric; chiral nematic; nematic; banana-shaped molecules; chirality

1. Introduction

Recently, a new class of nematic (N) phases has been discovered in liquid crystalline (LC) dimers and bent-core molecules (or banana-shaped molecules). The novel twist-bend nematic (N_{TB}) phase is an oblique helicoidal structure with a nanoscale pitch. It has been theoretically predicted almost 50 years ago by Meyer(*1*), but only recently was observed experimentally.(*2–22*) It was first identified for 1, 7-bis-4-(4-cyanobiphenyl) heptane, CB7CB,(*3*) and the N_{TB} phase was confirmed by freeze fracture transmission electron microscopy (FFTEM)(*5*) , NMR,(*6*) and X-ray scattering, etc.(*7*) After that, many studies have been conducted and the workshop on the N_{TB} phase has been held in 2016.(*23*) The research on the N_{TB} phase is getting active more and more.(*24, 25*)

The N_{TB} phase in achiral molecules, such as banana-shaped molecules, appears at the lower temperatures of a N phase(*6, 7*) and has the same director as an oblique helicoidal structure, which is induced by electric fields applying parallel to the pitch axis of a chiral nematic (N^*) phase.(*26–28*) It has been suggested that the spontaneous formation of such chiral systems from the achiral LC molecules is due to the conformational chirality within each molecules.(*29–32*) The N_{TB} phase is

*Corresponding author. Email: matuyama@bio.kyutech.ac.jp

ISSN: 0267-8292 print/ISSN 1366-5855 online

DOI: 10.1080/0267829YYxxxxxxxx
http://www.informaworld.com

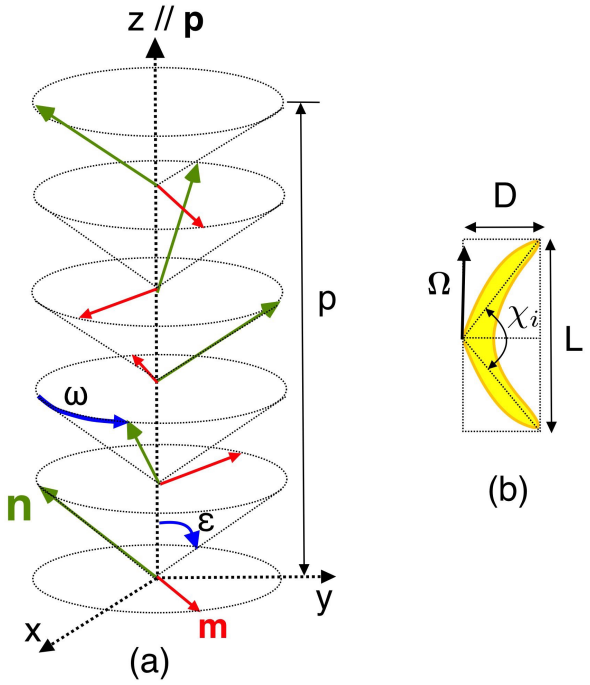

Figure 1. (color online) (a) Schematic representation of the director $\mathbf{n}$ of the N_{TB} phase with the cone angle ϵ between the director and the pitch axis direction $\mathbf{p}//z$: $\mathbf{p}$ and $\mathbf{n}$ are unit vectors parallel to the local director and to the helical axis, respectively, and the polarizing vector $\mathbf{m} = \mathbf{p} \times \mathbf{n}$. The angle ω is the azimuthal angle around the z axis. The figure shows one of the two degenerate helicoidal twists (right-($\omega < 0$) and left-handed ($\omega > 0$) helices). We have the N^* phase with $\epsilon = \pi/2$ and the N phase with $\epsilon = 0$. When $0 < \epsilon < \pi/2$, the N_{TB} appears.(b) Banana-shaped molecule of length L and diameter D with the molecular orientation vector $\mathbf{\Omega}$.

mainly formed in pure LC dimers having odd spacers(*3, 7*) and in binary mixtures of LC dimers.(*17–22*) Recent experiments for the binary mixtures of LC dimers have shown that the N_{TB} phase is formed directory from an isotropic (I) phase via a strong first-order phase transition,(*20*) in which the N_{TB} phase depends on not only temperature but also concentration. The motivation of this paper is to theoretically describe these binary mixtures of LC dimers.

In the N_{TB} phase, the director exhibits periodic twist and bend deformations forming an oblique heliconical helix with doubly degenerate domains having opposite handedness. Figure 1 shows a schematic representation of the director $\mathbf{n}$ of the N_{TB} phase. When the helix axis $\mathbf{p}$ is parallel to the z axis, the director is uniformly twisted along the z axis with the pitch length $p = 2\pi/q$, maintaining a constant cone angle $0 \leqslant \epsilon \leqslant \pi/2$ with the helix axis, and is given by

$$\mathbf{n}(z) = (\sin\epsilon\cos\omega(z), \sin\epsilon\sin\omega(z), \cos\epsilon), \tag{1}$$

where the azimuthal angle ω is given as a function of the position z: $\omega = qz$. The cone angle ϵ between the director and pitch axes is a constant and does not depend on the position z. Equation (1) can also describe a N phase when $\epsilon = 0$ and a N^* phase when $\epsilon = \pi/2$.

To describe the N_{TB} phase in achiral systems, Dozov(*33*) has shown that the bend elastic constant K_{33} become a negative value in bent-core LC molecules. Shamid et.al(*34, 35*) have also found that the bend-polarization coupling leads to a negative K_{33}. On the other hand, a quadratic elastic theory with a coupling between a nematic director and an extra director field parallel to the pitch axis of a N_{TB} phase leads to a non-negative elastic constant.(*36–39*) These theories demonstrate that the twist elastic constant K_{22} is always $K_{22} > K_{33}$ to derive

a stable N_{TB} phase. Molecular field approaches have also been proposed as generalized Maier-Saupe theory,(*40–43*) as well as Onsager-like theory.(*44*) Recently, we have presented the mean field theory to describe the N_{TB} phase for a pure banana-shaped molecule, in which we take into account the coupling between the director and pitch axis: director-pitch (DP) coupling, and described the N_{TB} phase depending on temperature and the coupling strength.(*39*) Our theory is consistent with the elastic theory for the N_{TB}.(*36–38*) However, the phase diagrams for the binary mixtures of LC dimers showing the N_{TB} phase have not been theoretically discussed, yet.

In this paper, we present a mean field theory to describe the N_{TB} phase in binary mixtures of banana-shaped LC molecules with $K_{22} > K_{33}$. Based on our previous theory(*39*) of the N_{TB} for a pure LC molecule, we extend it to the binary mixtures, in which we take into account the DP coupling. We derive the free energy of the binary mixtures of LC dimers and explore the N_{TB} phase, depending on temperature and concentration. We calculate the orientational order parameter S_i of the LC molecule $i(= A, B)$ and the order parameter $y(\equiv \sin^2\epsilon)$ of the N_{TB} phase as a function of the temperature and concentration. We also calculate the phase diagrams on the temperature-concentration plane, depending on the strength of the DP coupling, and find a various phase diagrams: the second-order $N - N_{TB}$ phase transition and the first-order $pN(I) - N$ and $pN(I) - N_{TB}$ phase transitions, etc. The theory shows good agreements with the experimental phase diagrams.

In Section 2, we introduce the free energy to describe the N_{TB} phase in the binary mixtures. In Section 3.1, we discuss phase transitions of the N_{TB} phase in the framework of a Landau expansion in a series of the order parameter y of the free energy. We show the numerical results of the phase diagrams in Section 3.3 and the comparisons of our theory with the experimental phase diagrams in Section 3.4.

2. Free energy of a binary mixture of LC molecules with chiral interactions

In this section, we introduce the free energy of a binary mixture of low-molecular weight LC molecules with chiral interactions.

Consider a binary mixture of LC molecules A and B. Let N_A be the number of the LC molecule A of the length L_A and diameter D and N_B be the number of the LC molecule B of the length L_B and diameter D. Let χ_i be the bend angle between two bent-core mesogens of the molecule i. We assume that the banana-shaped LC molecule is like a rodlike molecule with the length $L_i = 2D\tan(\chi_i/2)$ and the diameter D. We then have the ratio $n_i \equiv L_i/D = 2\tan(\chi_i/2)$. Note that we here consider $\pi/2 \ll \chi_i \ll \pi$ for the bend angle. The volume of the LC molecule A and that of B are given by $v_A = a^3 n_A$ and $v_B = a^3 n_B$, respectively, where we define $a^3 \equiv (\pi/4)D^3 \simeq D^3$. Let $\phi_A = v_A N_A/V$ and $\phi_B = v_B N_B/V$ be the volume fraction of the molecule A and B, respectively, where V is the volume of the system: $\phi_A + \phi_B = 1$.

The free energy of the mixtures consists of the following three terms:

$$F = F_{mix} + F_{ani} + F_{co}. \tag{2}$$

The first term in Equation (2) is the free energy of mixing for the binary mixture and can be given by Flory-Huggins theory for polymer blends:(*45, 46*)

$$f_{mix} \equiv a^3\beta F_{mix}/V = \frac{\phi_A}{n_A}\ln\phi_A + \frac{\phi_B}{n_B}\ln\phi_B + \chi_{FH}\phi_A\phi_B, \tag{3}$$

where χ_{FH} is the Flory-Huggins interaction parameter between LC molecules in an isotropic phase and $\beta \equiv 1/k_BT$; T is the absolute temperature, k_B is the Boltzmann constant. In the case of binary mixtures with a good solubility, we can take the interaction parameter of $\chi_{FH} = 0$.

The second term in Equation (2) shows the anisotropic free energy for liquid crystalline ordering. The configuration of a constituent molecule is characterized by its position vector $\mathbf{r}$ and its orientation unit vector $\mathbf{\Omega} = (\sin\theta\cos\varphi, \sin\theta\sin\varphi, \cos\theta)$, defined by a polar angle θ and an azimuthal angle φ, or solid angle $d\Omega(= \sin\theta d\theta d\varphi)$, in a fixed coordinate frame. Let $f_i(\mathbf{n}(\mathbf{r})\cdot\mathbf{\Omega})$ be the orientational distribution function of the constituent molecule $i(= A, B)$, where $\mathbf{n}(\mathbf{r})$ is the local director. It should be noted that the distribution function depends only on the relative angle between the local director $\mathbf{n}(\mathbf{r})$ and the molecular orientation vector $\mathbf{\Omega}$. The anisotropic part of the free energy in the second virial approximation can be given by(*46*)

$$\begin{aligned}\beta F_{ani} = &\sum_{i=A,B}\rho_i\int f_i(\mathbf{n}(\mathbf{r})\cdot\mathbf{\Omega})\ln 4\pi f_i(\mathbf{n}(\mathbf{r})\cdot\mathbf{\Omega})d\mathbf{r}d\Omega\\ &+\frac{1}{2}\sum_{i,j=A,B}\rho_i\rho_j\int f_i(\mathbf{n}(\mathbf{r}_1)\cdot\mathbf{\Omega}_1)f_j(\mathbf{n}(\mathbf{r}_2)\cdot\mathbf{\Omega}_2)\\ &\times\beta U_{ij}(\mathbf{r}_1,\mathbf{\Omega}_1;\mathbf{r}_2,\mathbf{\Omega}_2)d\mathbf{R},\end{aligned} \tag{4}$$

where $d\mathbf{R} \equiv d\mathbf{r}_1 d\mathbf{r}_2 d\Omega_1\Omega_2$, $\rho_i = N_i/V$ is the number density of the LC molecule i. The first term in Equation (4) shows the entropy changes due to orientational ordering and U_{ij} is the orientation-dependent intermolecular potential between two particles i and j $(i, j = A, B)$. The lowest-order contributions to the interaction potential are given in a series of the Legendre polynomials:(*47–52*)

$$\begin{aligned}U_{ij}(\mathbf{r}_1,\mathbf{\Omega}_1;\mathbf{r}_2,\mathbf{\Omega}_2) = &U_{ij,1}(\mathbf{r}_{12})(\mathbf{\Omega}_1\times\mathbf{\Omega}_2\cdot\hat{\mathbf{r}}_{12})P_1(\mathbf{\Omega}_1\cdot\mathbf{\Omega}_2)\\ &+U_{ij,2}(\mathbf{r}_{12})P_2(\mathbf{\Omega}_1\cdot\mathbf{\Omega}_2),\end{aligned} \tag{5}$$

where $\mathbf{r}_{12} = \mathbf{r}_2 - \mathbf{r}_1$ and $\hat{\mathbf{r}}_{12}(= \mathbf{r}_{12}/|\mathbf{r}_{12}|)$ is a unit vector. The potential $U_{ij,1}$ shows the chiral interaction between LC molecules and the pseudoscalar term $\mathbf{\Omega}_1\times\mathbf{\Omega}_2\cdot\hat{\mathbf{r}}_{12}$ represents scalars coupling between orientational and spatial variables. The potential $U_{ij,2}$ shows the intermolecular potential for a nematic phase, which has been used in Maier-Saupe(*53*) and Onsager models.(*54*) As usual we here employ a simple square well interaction potential energy with a short range $d_0(\simeq D)$ on the order of the molecule.(*51*) We then define a numerical parameter $c_{ij} \equiv -U_{ij,1}/k_BT$ for a chiral pseudoscalar interaction parameter between LC molecules and $\nu_{ij} \equiv -U_{ij,2}/k_BT(> 0)$ for a nematic interaction (or Maier-Saupe) parameter. The interaction parameter $\nu_{ij} > 0$ corresponds to the orientational-dependent (Maier-Saupe) interaction parameter between the LC molecules i and j. The larger values of ν_{ij} imply that the two molecules i and j prefer to be parallel to each other and a N phase tends to be more stable in the mixture. The chiral interaction parameter c_{ij} corresponds to the strength of the chirality between the LC molecules i and j. The larger values of c_{ij} show stronger chirality (or twist interaction) between the LC molecules i and j and a twist distortion, or a N^* phase, tends to be more stable in the mixture.

Using the orientational distribution function $f_i(\mathbf{n}(\mathbf{r})\cdot\mathbf{\Omega})$, the second rank order

parameter tensor $\mathcal{Q}^{(i)}_{\alpha\beta}(\mathbf{r})$ is given by (*55*)

$$\mathcal{Q}^{(i)}_{\alpha\beta}(\mathbf{r}) = \int f_i(\mathbf{n}(\mathbf{r})\cdot\mathbf{\Omega})\big(\frac{3}{2}\Omega_\alpha\Omega_\beta - \frac{1}{2}\delta_{\alpha\beta}\big)d\Omega$$
$$= \big\langle \frac{3}{2}\Omega_\alpha\Omega_\beta - \frac{1}{2}\delta_{\alpha\beta}\big\rangle, \tag{6}$$

where Ω_α is the Cartesian component of the molecular orientation vector $\mathbf{\Omega}$ at a position $\mathbf{r}$ and $\delta_{\alpha\beta}$ is the Kronecker delta function.

Using Equation (6), the average over Ω_1 and Ω_2 in Equation (4) yields(*51*)

$$\iint f_i(\mathbf{n}(\mathbf{r}_1)\cdot\mathbf{\Omega}_1) f_j(\mathbf{n}(\mathbf{r}_2)\cdot\mathbf{\Omega}_2)(\mathbf{\Omega}_1\times\mathbf{\Omega}_2\cdot\hat{\mathbf{r}}_{12})P_1(\mathbf{\Omega}_1\cdot\mathbf{\Omega}_2)d\Omega_1 d\Omega_2$$
$$= \frac{4}{9}\epsilon_{\alpha\beta\gamma}\hat{r}_{12,\alpha}\mathcal{Q}^{(i)}_{\beta\mu}(\mathbf{r}_1)\mathcal{Q}^{(j)}_{\gamma\mu}(\mathbf{r}_2), \tag{7}$$

and

$$\iint f_i(\mathbf{n}(\mathbf{r}_1)\cdot\mathbf{\Omega}_1) f_j(\mathbf{n}(\mathbf{r}_2)\cdot\mathbf{\Omega}_2)P_2(\mathbf{\Omega}_1\cdot\mathbf{\Omega}_2)d\Omega_1 d\Omega_2$$
$$= \frac{2}{3}\mathcal{Q}^{(i)}_{\alpha\beta}(\mathbf{r}_1)\mathcal{Q}^{(j)}_{\alpha\beta}(\mathbf{r}_2), \tag{8}$$

where $\epsilon_{\alpha\beta\gamma}$ is Levi-Civita antisymmetric tensor of the third rank and $\hat{r}_{12,\alpha}$ is the α component of the unit vector $\hat{\mathbf{r}}_{12}$.

We here assume that the $\mathcal{Q}_{\alpha\beta}(\mathbf{r}_2)$ does not change appreciably over the range of the potential and can be expanded in the Taylor series:

$$\mathcal{Q}_{\alpha\beta}(\mathbf{r}_2) = \mathcal{Q}_{\alpha\beta}(\mathbf{r}_1+\mathbf{r}_{12})$$
$$= \mathcal{Q}_{\alpha\beta}(\mathbf{r}_1) + r_\kappa\partial_\kappa\mathcal{Q}_{\alpha\beta}(\mathbf{r}_1) + \frac{1}{2}r_\kappa r_\mu\partial_\kappa\partial_\mu\mathcal{Q}_{\alpha\beta}(\mathbf{r}_1), \tag{9}$$

where $r_\kappa \equiv r_{12,\kappa}$ is the the κ component of the position vector $\mathbf{r}_{12}$ and $\partial_\mu = \partial/\partial\mu$ is the first spatial derivative of the tensor order parameter $(\kappa,\mu = x,y,z)$.

Substituting Equation (9) into (7) and (8), the anisotropic free energy of the binary mixtures with chiral interactions can be expressed as(*39, 51*)

$$a^3\beta F_{ani}/V = \sum_{i=A,B}\frac{\phi_i}{n_i}\int f_i(\mathbf{n}(\mathbf{r})\cdot\mathbf{\Omega})\ln 4\pi f_i(\mathbf{n}(\mathbf{r})\cdot\mathbf{\Omega})d\Omega$$
$$+\sum_{i,j=A,B}\Big[-\frac{1}{2}\nu_{ij}\phi_i\phi_j\frac{2}{3}\mathcal{Q}^{(i)}_{\alpha\beta}(\mathbf{r})\mathcal{Q}^{(j)}_{\alpha\beta}(\mathbf{r})$$
$$+\frac{1}{2}\nu_{ij}\phi_i\phi_j\frac{1}{9}\partial_\mu\mathcal{Q}^{(i)}_{\alpha\beta}(\mathbf{r})\partial_\mu\mathcal{Q}^{(j)}_{\alpha\beta}(\mathbf{r})d_0^2$$
$$-\frac{1}{2}c_{ij}\phi_i\phi_j\frac{4}{9}\epsilon_{\alpha\beta\gamma}\mathcal{Q}^{(i)}_{\mu\beta}(\mathbf{r})\partial_\alpha\mathcal{Q}^{(j)}_{\mu\gamma}(\mathbf{r})d_0\Big]. \tag{10}$$

It is easy to develop Equation (10) for multi-component systems.

The tensor order parameter of the LC molecule i is given by:(*55*)

$$\mathcal{Q}^{(i)}_{\alpha\beta}(\mathbf{r}) = S_i\left(\frac{3}{2}n_\alpha(\mathbf{r})n_\beta(\mathbf{r}) - \frac{1}{2}\delta_{\alpha\beta}\right), \tag{11}$$

where n_α is the $\alpha(= x, y, z)$ component of the director $\mathbf{n}$ and S_i is the scalar orientational order parameter of the molecule i:

$$S_i = \int P_2(\mathbf{n}(\mathbf{r})\cdot\mathbf{\Omega})f_i(\mathbf{n}(\mathbf{r})\cdot\mathbf{\Omega})d\Omega. \tag{12}$$

The last term in Equation (2) shows the DP coupling between the director $\mathbf{n}$ and the pitch field $\mathbf{p} = (0, 0, 1)$ of the N_{TB} phase. Using the tensor order parameter (Equation (11)) and the director $\mathbf{n}$, it is given by(*37, 39*)

$$\begin{aligned} a^3\beta F_{co}/V &= -\sum_{i=A,B}\gamma_i\phi_i p_\alpha \mathcal{Q}^{(i)}_{\alpha\beta}(\mathbf{r})p_\beta, \\ &= -(\gamma_A\phi_A S_A + \gamma_B\phi_B S_B)(1 - \frac{3}{2}y), \end{aligned} \tag{13}$$

where p_α is the $\alpha(= x, y, z)$ component of the pitch field $\mathbf{p}$ and γ_i is the dimensionless parameter denoted the strength of the intrinsic coupling between $\mathbf{p}$ and $\mathcal{Q}^{(i)}_{\alpha\beta}$ of the LC molecule i. This coupling term γ_i has been discussed in the elastic theory of the N_{TB} phase and gives rise to a local oblique twisting power.(*37–39*) For larger values of γ_i, the director $\mathbf{n}$ tends to align parallel to the pitch $\mathbf{p}$, namely, the system tends to be a homogeneous N phase. This term also mathematically has the same form with the interaction between the director and the external electric field.(*27, 28*)

Substituting Equation (11) into Equations (10) and (13), we obtain the free energy of LC phases:(*39*)

$$F_{LC} \equiv F_{ani} + F_{co} = F_{nem} + F_{dis}, \tag{14}$$

where we have separated the anisotropic free energy into two parts. One is the nematic free energy of Maier-Saupe type(*53*):

$$\begin{aligned} f_{nem} \equiv a^3\beta F_{nem}/V = &\sum_{i=A,B}\frac{\phi_i}{n_i}\int f_i(\mathbf{n}(\mathbf{r})\cdot\mathbf{\Omega})\ln 4\pi f_i(\mathbf{n}(\mathbf{r})\cdot\mathbf{\Omega})d\Omega \\ &-\frac{1}{2}\nu_A\phi_A^2 S_A^2 - \nu_{AB}\phi_A\phi_B S_A S_B \\ &-\frac{1}{2}\nu_B\phi_B^2 S_B^2 - (\gamma_A\phi_A S_A + \gamma_B\phi_B S_B), \end{aligned} \tag{15}$$

where we write $\nu_A \equiv \nu_{AA}$ and $\nu_B \equiv \nu_{BB}$ for simplicity. The other is the distortion

free energy due to the spatial variation of the director for N^* and N_{TB} phases:

$$f_{dis} \equiv a^3 \beta F_{dis}/V = \frac{1}{2}\nu_A \phi_A^2 S_A^2 g_A(y,Q) + \nu_{AB}\phi_A\phi_B S_A S_B g_{AB}(y,Q) + \frac{1}{2}\nu_B \phi_B^2 S_B^2 g_B(y,Q) + \frac{3}{2}(\gamma_A \phi_A S_A + \gamma_B \phi_B S_B)y, \quad (16)$$

where we define the functions g_i as a function of two order parameters: the pitch wavenumber $Q \equiv qd_0$ and the order parameter $y \equiv \sin^2\epsilon$ of the N_{TB} phase,

$$g_A(y,Q) \equiv \frac{1}{2}(\tilde{k}_2 - \tilde{k}_3)Q^2 y^2 + \big(\frac{1}{2}\tilde{k}_3 Q - \tilde{k}_2 Q_A\big)Qy, \quad (17)$$

$$g_{AB}(y,Q) \equiv \frac{1}{2}(\tilde{k}_2 - \tilde{k}_3)Q^2 y^2 + \big(\frac{1}{2}\tilde{k}_3 Q - \tilde{k}_2 Q_{AB}\big)Qy, \quad (18)$$

and

$$g_B(y,Q) \equiv \frac{1}{2}(\tilde{k}_2 - \tilde{k}_3)Q^2 y^2 + \big(\frac{1}{2}\tilde{k}_3 Q - \tilde{k}_2 Q_B\big)Qy, \quad (19)$$

with $Q_A \equiv c_A/\nu_A$, $Q_B \equiv c_B/\nu_B$ and $Q_{AB} \equiv c_{AB}/\nu_{AB}$ (Note that the notations Q_A and Q_{AB} are described as Q_0 and α_x in the previous paper, respectively (*51*)). The values of $\tilde{k}_2$ and $\tilde{k}_3$ correspond to the dimensionless elastic constants of the twist $(\mathbf{n}\cdot\nabla\times\mathbf{n})^2$ and bend $(\mathbf{n}\times\nabla\times\mathbf{n})^2$ distortions, respectively.(*39*) We assume that these constants are normalized by the typical value ($\sim 10^{-6}$ dyn) of the elastic constant of a pure LC molecule ($\phi_i = 1$) with $S_i = 1$. When $\phi_i = 1$ ($i = A$ or B) and $y = 1$, the function g_i has a minimum at $Q = Q_i$. Apparently, the value of Q_i corresponds to the dimensionless wavenumber of the N^* phase in the pure LC molecule i and is given by $Q_i(\equiv c_i/\nu_i) = d_0 q_{0i}$. When $y = 0$ (or a N phase), we have $f_{dis} = 0$.

2.1. *Distribution functions in an equilibrium state*

The orientational distribution function $f_A(\mathbf{n}(\mathbf{r})\cdot\mathbf{\Omega})$ of the LC molecule A and $f_B(\mathbf{n}(\mathbf{r})\cdot\mathbf{\Omega})$ of the component B are determined by the free energy (Equation (14)) with respect to these functions: $(\delta F_{LC}/\delta f_i) = 0$, under the normalization condition:

$$\int f_i(\mathbf{n}(\mathbf{r})\cdot\mathbf{\Omega})d\Omega = 1. \quad (20)$$

We then obtain

$$f_A(x) = \frac{1}{Z_A}\exp\big[\Gamma_A P_2(x)\big], \quad (21)$$

and

$$f_B(x) = \frac{1}{Z_B}\exp\big[\Gamma_B P_2(x)\big], \quad (22)$$

where we define

$$\Gamma_A \equiv n_A \Big[\nu_A \phi_A S_A \big(1 - g_A(y,Q)\big) + \nu_{AB} \phi_B S_B \big(1 - g_{AB}(y,Q)\big) + \gamma_A (1 - \frac{3}{2} y) \Big], \tag{23}$$

and

$$\Gamma_B \equiv n_B \Big[\nu_B \phi_B S_B \big(1 - g_B(y,Q)\big) + \nu_{AB} \phi_A S_A \big(1 - g_{AB}(y,Q)\big) + \gamma_B (1 - \frac{3}{2} y) \Big]. \tag{24}$$

The constants Z_A and Z_B are determined by the normalization condition (Equation (20)) as $Z_A = 4\pi I_0(S_A, S_B)$ and $Z_B = 4\pi J_0(S_A, S_B)$, respectively. The functions I_m and J_m are defined as:

$$I_m(S_A, S_B) \equiv \int_0^1 [P_2(x)]^m \exp\big[\Gamma_A P_2(x)\big] dx, \tag{25}$$

$$J_m(S_A, S_B) \equiv \int_0^1 [P_2(x)]^m \exp\big[\Gamma_B P_2(x)\big] dx, \tag{26}$$

respectively, where $m = 0, 1, 2 \cdots$.

Substituting Equations (21) and (22) into (12), the scalar orientational order parameters S_A and S_B can be determined by the two coupled-self-consistent equations:

$$S_A = I_1(S_A, S_B)/I_0(S_A, S_B), \tag{27}$$

and

$$S_B = J_1(S_A, S_B)/J_0(S_A, S_B). \tag{28}$$

Using the distribution functions (21) and (22), the free energy (Equation (14)) of the LC phases is given by

$$\begin{aligned} a^3 \beta F_{LC}/V = & \frac{1}{2} \nu_A \phi_A^2 S_A^2 \big(1 - g_A(y,Q)\big) \\ & + \nu_{AB} \phi_A \phi_B S_A S_B \big(1 - g_{AB}(y,Q)\big) \\ & + \frac{1}{2} \nu_B \phi_B^2 S_B^2 \big(1 - g_B(y,Q)\big) \\ & - \frac{\phi_A}{n_A} \ln I_0 - \frac{\phi_B}{n_B} \ln J_0. \end{aligned} \tag{29}$$

When $y = 0$, Equation (29) results in the nematic free energy of a binary mixture of LC molecules.(*46*) The total free energy (F) is given by the sum of Equations (3) and (29) .

2.2. *Determination of the order parameter y and pitch length p*

We here derive the equilibrium value y^* and pitch wavenumber Q^* in a thermal equilibrium state. The procedure is to minimize the distortion free energy f_{dis} (Equation (16)), with respect to y and Q: $(\partial f_{dis}/\partial y)_{Q,S_i} = 0$ and $(\partial f_{dis}/\partial Q)_{y,S_i} = 0$. It is convenient to rewrite the distortion free energy f_{dis} as follows:

$$f_{dis} = \frac{1}{2}\nu_A\big(\phi_A^2 S_A^2 + 2\epsilon_n \phi_A\phi_B S_A S_B + \epsilon_{nB}\phi_B^2 S_B^2\big) g(y, Q; \eta), \tag{30}$$

where we define the distortion function:

$$g(y, Q; \eta) \equiv \frac{1}{2}(\tilde{k}_2 - \tilde{k}_3)Q^2 y^2 + \left[\big(\frac{1}{2}\tilde{k}_3 Q - \tilde{k}_2\eta_0 Q_A\big)Q + \eta\right] y, \tag{31}$$

with the symbols

$$\eta_0 \equiv \frac{\phi_A^2 S_A^2 + 2\epsilon_x\phi_A\phi_B S_A S_B + \epsilon_{xB}\phi_B^2 S_B^2}{\phi_A^2 S_A^2 + 2\epsilon_n\phi_A\phi_B S_A S_B + \epsilon_{nB}\phi_B^2 S_B^2}, \tag{32}$$

$$\eta \equiv \frac{3(\gamma_A\phi_A S_A + \gamma_B\phi_B S_B)}{\nu_A(\phi_A^2 S_A^2 + 2\epsilon_n\phi_A\phi_B S_A S_B + \epsilon_{nB}\phi_B^2 S_B^2)}, \tag{33}$$

and the numerical parameters: $\epsilon_n \equiv \nu_{AB}/\nu_A$, $\epsilon_{nB} \equiv \nu_B/\nu_A$, $\epsilon_x \equiv c_{AB}/c_A$, and $\epsilon_{xB} \equiv c_B/c_A$. Note that the η and η_0 are given as a function of the concentration and the orientational order parameter S_i. When $\phi_A = 1$, the value of η results in that of the pure LC molecule A.(*39*) The value of η_0 contains the chiral interaction parameters: ϵ_x and ϵ_{xB} in the numerator, and the larger values of η_0 favor a N^* phase. On the other hand, the value of η contains the director-pitch coupling parameters: γ_A and γ_B, and the larger values of η favor a N_{TB} or N phase.

Using Equation (31), we obtain the equilibrium value

$$y^*(\equiv \sin^2\epsilon) = \frac{\tilde{k}_2\eta_0 Q_A/Q^* - \tilde{k}_3}{\tilde{k}_2 - \tilde{k}_3}, \tag{34}$$

for the cone angle and

$$Q^* = \pm\sqrt{\frac{2\eta}{\tilde{k}_3}}, \tag{35}$$

for the pitch wavenumber $Q^*(\propto 1/p)$. The sign $(+)$ shows the left-handed helix with $Q_A > 0$ and the sign $(-)$ is the right-handed helix with $Q_A < 0$. In the N_{TB} phases, both $(+)$ and $(-)$ twist appear in a sample with the same probability, because the free energy has the same value. This result is in agreement with the experiments(*5, 11*) and the elastic theory.(*37*) We can also derive the effective twist K_{22} and bend K_{33} elastic constant of the twist $(\mathbf{n}\cdot\nabla\times\mathbf{n} + q_{0A})^2$ and bend $(\mathbf{n}\times\nabla\times\mathbf{n})^2$ distortions, respectively:(*39*)

$$aK_{22}/k_BT = \frac{1}{2}\big(\nu_A S_A^2\phi_A^2 + 2\nu_{AB}S_A S_B\phi_A\phi_B + \nu_B S_B^2\phi_B^2\big)\tilde{k}_2, \tag{36}$$

and

$$aK_{33}/k_BT = \frac{1}{2}\big(\nu_A S_A^2\phi_A^2 + 2\nu_{AB}S_AS_B\phi_A\phi_B + \nu_B S_B^2\phi_B^2\big)\tilde{k}_3. \tag{37}$$

The ratio of the two elastic constants is given by a constant: $K_{22}/K_{33} = \tilde{k}_2/\tilde{k}_3$=const.(*39*)

The values of y^* and Q^* must be a minimum of the free energy (Equation (30)). The minimum of the free energy function f_{dis}, or minimum of the distortion function g, which depends on y and Q variables occurs when the Hessian is positive definite matrix:

$$\begin{aligned}|H(y^*,Q^*)| &= \begin{vmatrix} \frac{\partial^2 f_{dis}}{\partial y^2} & \frac{\partial^2 f_{dis}}{\partial y\partial Q} \\ \frac{\partial^2 f_{dis}}{\partial Q\partial y} & \frac{\partial^2 f_{dis}}{\partial Q^2} \end{vmatrix} \\ &= \frac{1}{2}\nu_A(\phi_A^2S_A^2 + 2\epsilon_n\phi_A\phi_BS_AS_B + \epsilon_{nB}\phi_B^2S_B^2)\tilde{k}_3(\tilde{k}_2-\tilde{k}_3)Q^{*2}y^* \\ &= 3\tilde{k}_3\big[\gamma_BS_B + (\gamma_AS_A - \gamma_BS_B)\phi_A\big]\left(\frac{K_{22}}{K_{33}} - 1\right)y^* > 0. \end{aligned} \tag{38}$$

We then find the stable N_{TB} phase appears when $\tilde{k}_2 > \tilde{k}_3 > 0$, or $K_{22} > K_{33} > 0$, with $\gamma_AS_A > 0$ and $\gamma_BS_B > 0$ because of $y^* > 0$. In this paper, we focus on $S_A > 0$ and $S_B > 0$.

3. Numerical Results and Discussion

In this section we show the numerical results for the phase transitions of the N_{TB} phase (Sec. 3.1) and the phase diagrams (Sec. 3.2). In the following, we chose the (+) sign ($Q_i > 0$, $Q > 0$) for chirality without loss of generality. The same discussions are also valid for the (−) sign ($Q_i < 0$, $Q < 0$).

3.1. *Phase transitions between N, N*, and N_{TB} phases*

In this subsection, we examine how Equation (30) describes phase transitions between N_{TB}, N^*, and N phases. In the following, we set $\tilde{k}_2/\tilde{k}_3(= K_{22}/K_{33}) = 5$ and $\tilde{k}_3$=0.1 as a typical example. The pitch wavenumber $Q_A(= 2\pi d_0/p_0)$ can be estimated as $Q_A \simeq 0.1$ for the typical pitch length $p_0 \sim$10 nm and $d_0 = 0.5$ nm. The distortion free energy (Equation (30)) is the quadratic function of y: $g = Ay^2 + By$, and can be easily understood in the framework of a Landau expansion in a series of y. The same arguments have been used in the elastic theory for the N_{TB} phase.(*37–39*)

Figure 2 shows the equilibrium value of the order parameter y (Equation (34)) as a function of η for various values of η_0. With increasing η, the order parameter continuously decreases from 1 at $\eta = \eta_{CT}$ to 0 at $\eta = \eta_{TN}$. The phase transitions $N^* - N_{TB}$ and $N_{TB} - N$ are the second-order transitions because the value of the order parameter y continuously changes. The $N^* - N_{TB}$ transition takes place at $y^* = 1$. Using Equations (34) and (35), we obtain the critical value of the $N^* - N_{TB}$ transition:

$$\eta_{CT} = \frac{\tilde{k}_3}{2}(\eta_0 Q_A)^2, \tag{39}$$

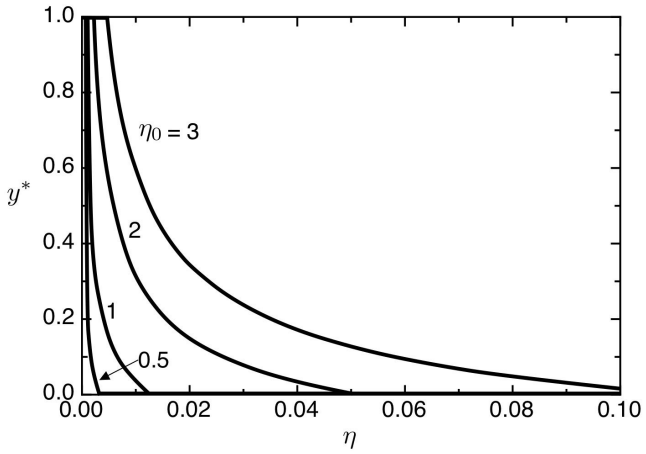

Figure 2. Equilibrium values of the order parameter y (Equation (34)) as a function of η for various values of η_0. With increasing η, the order parameter continuously decreases from 1 at $\eta = \eta_{CT}$ to 0 at $\eta = \eta_{TN}$.

at which we have $Q^*_{CT} = \pm\eta_0 Q_A$. The phase transition between N_{TB} and N phases takes place at $y^* = 0$. Using Equations (34) and (35), we obtain the critical value of the $N_{TB} - N$ transition:

$$\eta_{TN} = \frac{(\eta_0 Q_A)^2}{2}\frac{\tilde{k}_2^2}{\tilde{k}_3} = (\frac{\tilde{k}_2}{\tilde{k}_3})^2 \eta_{CT}, \tag{40}$$

where we have $Q^*_{TN} = (\tilde{k}_2/\tilde{k}_3)\eta_0 Q_A$. The value of η, Equation (33), is important to discuss the phase transitions.

We here summarize:

(1)When $0 < \eta < \eta_{CT}$, we have the N^* phase with $y^* = 1$ and the wavenumber of the N^* phase is given by

$$Q_{N^*} = \eta_0 Q_A. \tag{41}$$

(2) When $\eta_{CT} < \eta < \eta_{TN}$, the N_{TB} phase appears. The wavenumber of the N_{TB} is given by Equation (35). The order parameter y^* of the N_{TB} phase is given by Equation (34).

(3)When $\eta_{TN} < \eta$, the distortion function f_{dis} has a minimum at $y = 0$ and then either N or I phase appears. When $\gamma_i = 0$, we have a disordered isotropic phase at higher temperatures. When $\gamma_i \neq 0$, we have a para-nematic (pN) phase with very small orientational order S_i and then the pN phase is almost an I phase. In this regard, we may write $pN(I)$ instead of pN.

The values of η and η_0 depend on the concentration ϕ_A and the temperature through the order parameters S_A and S_B. The orientational order parameters S_A and S_B can be numerically solved from Equations (27) and (28).

3.2. *Phase diagrams including I, N, N*, and N_{TB} phases of a pure LC molecule.*

In this subsection, we show the phase diagram on the temperature-concentration plane for a pure banana-shaped LC molecule $i(=A$ or $B)$: $\phi_i = 1$, with $n_i = 4$ corresponding to the bend angle $\chi_i = 127°$.(*39*) We here define the temperature parameter $\tau_i(\propto T)$:(*55*)

$$\tau_i \equiv T/T_{NI,i} = 4.55/(n_i \nu_i), \tag{42}$$

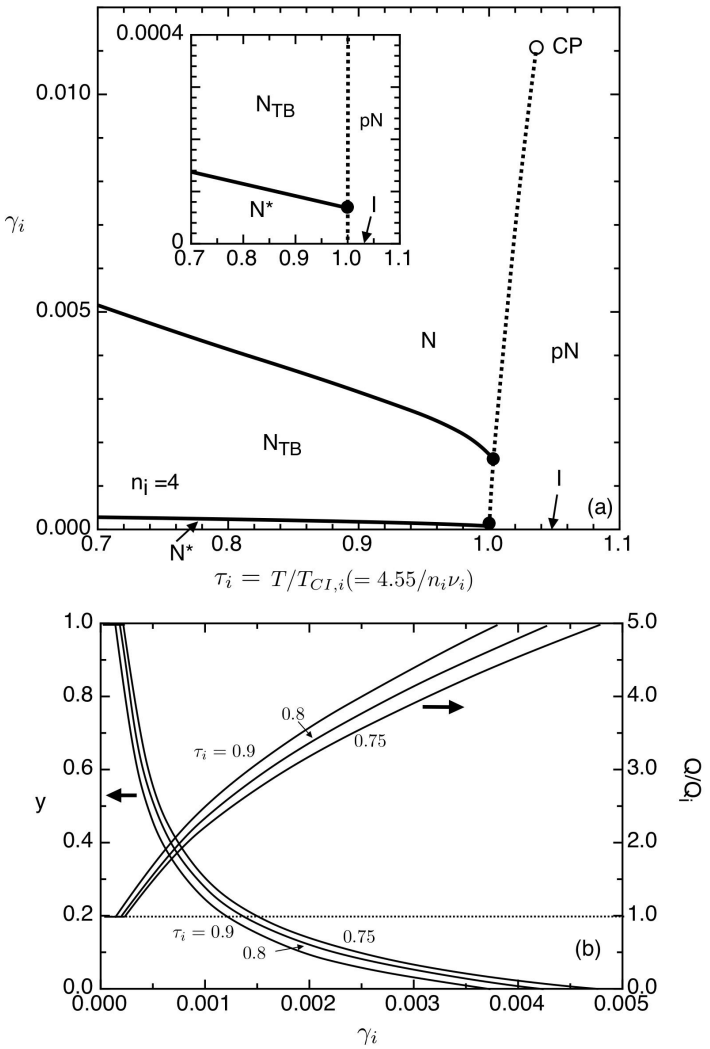

Figure 3. (a) Phase diagram on the coupling strength γ_i and temperature $T/T_{CI,i}$ plane for the pure LC molecule $i(= A, B)$ with $n_i = 4$ and $Q_i = 0.1$. The solid curves show the second-order phase transitions: $N - N_{TB}$ and $N_{TB} - N^*$ phase transitions. The dotted-curves show the first-order phase transitions: $pN - N$, $pN - N_{TB}$, and $pN - N^*$ phase transitions. The closed circles show the tricritical point and the open circle shows the critical point (CP). The inset shows the phase diagram at the weak field γ_i. (b) Order parameter $y(= \sin^2 \epsilon)$ (right) and the pitch wavenumber Q/Q_i (left) of the N_{TB} phase plotted against the DP coupling γ_i for $T/T_{CI,i} = 0.9$, 0.8, and 0.75.

where $T_{NI,i}$ shows the $N-I$ phase transition temperature of the pure LC molecule i. For the numerical calculations, we use $\nu_i = 4.55/(n_i\tau_i)$.

Figure 3(a) shows the phase diagram on the DP coupling parameter γ_i $(i = A, B)$ and the reduced-temperature $T/T_{CI,i}$ plane for the pure LC molecule of $n_i = 4$ and $Q_i = 0.1$.(*39*) The temperature is normalized by the $N^* - I$ phase transition temperature $T_{CI,i}$ at $\gamma_i = 0$ and then the $N^* - I$ transition takes place at $\tau_i(\equiv T/T_{CI,i}) = 1$.(*51*) The solid curves show the second-order phase transitions: $N - N_{TB}$ and $N_{TB} - N^*$ transitions. The dotted-curves show the first-order phase transitions: $pN - N$, $pN - N_{TB}$, and $I(pN) - N^*$ transitions. The inner phase diagram is an enlarged view for small values of γ_i. Note that the pN phase has a very small orientational order for small γ_i and then it is experimentally an isotropic phase. The orientational order parameters S_i jump at the first-order phase transition points. The open circle shows the critical point (CP), which has been discussed in nematic liquid crystals under an external field(*56, 57*) and surface-aligned nematic films.(*58, 59*) We also find two tricritical points (TCPs), closed

circles, at which the second-order phase transition line meets the first-order one and three phases coexist. We find that the N_{TB} phase exists between the N and N^* phases and always appears at the lower temperatures of the N phase. This is consistent with the experiment of achiral systems.(*7*) The upper critical field γ_i^h of the $N - N_{TB}$ phase transition increases with decreasing temperature. The lower critical field γ_i^l slightly increases with decreasing temperature and the N_{TB} appears between the N^* and pN phases as a function of the temperature. The N_{TB} phase always appears at the higher temperatures of the N^* phase with small γ_i, although it has not experimentally observed yet. When the coupling strength γ_i is very small, we have the first-order $pN - N^*$ phase transition at $T/T_{CI,i} \simeq 1$. When $\gamma_i^l (\simeq 0.0001) < \gamma_i < \gamma_i^h (\simeq 0.0017)$ between two TCPs, we have the first-order $pN - N_{TB}$ phase transition. As the coupling γ_i increases, the temperature of the first-order $pN - N$ transition slightly increases toward the CP temperature. When the value of γ_i is larger than that of the CP, the orientational order parameter S_i continuously changes and the first-order $pN - N$ transition disappears.(*39*) As the value of n_i increases, the N_{TB} phase shifts to the higher temperatures and the value of the upper critical field γ_i^h increases. Figure 3(b) shows the order parameter $y(= \sin^2 \epsilon)$, or cone angle, and the pitch wavenumber Q/Q_i of the N_{TB} phase as a function of the director-pitch coupling γ_i for $T/T_{CI,i} = 0.9$, 0.8, and 0.75. The value of y decreases with increasing the coupling strength γ_i and the pitch wavenumber increases. For the pure LC molecules $\phi_A = 1$, we have $\eta_0 = 1$ in Equation (32). Using Equation (40), the pitch wavenumber at the $N^* - N_{TB}$ transition is given by $Q_{TN}^*/Q_A = (\tilde{k}_2/\tilde{k}_3)$=5, where we have $y = 0$.

In this paper, we do not take into account chiral smectic C (S_c^*) phases of achiral LC molecules.(*60*) The N^* phase appeared at the weak coupling γ_i may be the S_c^* phases. However, it can be understood that most of the banana-shaped LC molecule capable to form the N_{TB} phase has a nonzero $\gamma_i (> \gamma_i^l)$.

3.3. *Phase diagrams for binary mixtures of banana-shaped LC molecules.*

In this subsection, we show some phase diagrams of binary mixtures of banana-shaped LC molecules. Before that, we summarize the numerical parameters.

Using Equation (42), we define the ratio $\tilde{T}$ between two transition temperatures of the pure LC molecules:

$$\tilde{T} \equiv \frac{T_{NI,B}}{T_{NI,A}} = \frac{n_B \nu_B}{n_A \nu_A} = \epsilon_{nB} \left(\frac{n_B}{n_A} \right). \tag{43}$$

Then the parameter $\epsilon_{nB} (\equiv \nu_B/\nu_A)$ is given by

$$\epsilon_{nB} = \tilde{T} \left(\frac{n_A}{n_B} \right), \tag{44}$$

and $\nu_B = \epsilon_{nB} \nu_A$. We here assume that the nematic interaction ν_{AB} between the dissimilar molecules can be proportional to the square root of the product of ν_A and ν_B:(*61*)

$$\tilde{\nu} \equiv \frac{\nu_{AB}}{\sqrt{\nu_A \nu_B}}, \tag{45}$$

where $\tilde{\nu}$ is the constant characterizing the relative strength of the nematic interaction of the dissimilar LC molecules to that of the same LC molecules. The dependence of phase behavior for nematic binary mixtures on the parameter $\tilde{\nu}$ has

been discussed in details.(*61*) The smaller $\tilde{\nu}$ values imply that the N phase tends to be more stable in their pure N phase than in the mixed state, and vice versa. Using Equations (42), (43), and (45), the nematic interaction parameter between the dissimilar molecules is given by

$$\epsilon_n \equiv \nu_{AB}/\nu_A = \tilde{\nu}\sqrt{\epsilon_{nB}} = \tilde{\nu}\sqrt{\tilde{T}\left(\frac{n_A}{n_B}\right)}. \tag{46}$$

Similarly, for the chiral interaction c_{AB} between the dissimilar molecules, we put

$$\tilde{c} = \frac{c_{AB}}{\sqrt{c_A c_B}}, \tag{47}$$

where $\tilde{c}$ is the constant characterizing the relative strength of the chiral interaction of the dissimilar LC molecules to that of the same LC molecules. We then obtain the chiral interaction parameter

$$\epsilon_x \equiv c_{AB}/c_A = \tilde{c}\sqrt{\epsilon_{xB}}, \tag{48}$$

where the chiral parameter ϵ_{xB} is given by

$$\epsilon_{xB} \equiv c_B/c_A = \epsilon_{nB}\left(\frac{Q_B}{Q_A}\right) = \tilde{T}\left(\frac{n_A}{n_B}\right)\left(\frac{Q_B}{Q_A}\right). \tag{49}$$

Using ϵ_n and ϵ_x, we have

$$Q_{AB}(\equiv c_{AB}/\nu_{AB}) = (\epsilon_x/\epsilon_n)Q_A. \tag{50}$$

We here summarize the numerical parameters:

- $n_i(\equiv L_i/D = 2\tan(\chi_i/2))$ is the axial ratio of the LC molecule i with the bend angle χ_i.
- $Q_i(\equiv c_i/\nu_i)$ is the pitch wavenumber of the LC molecule i and is on the order of $\sim$0.1 (see Section 3.1). It also means the ratio between the strength of chirality and that of nematic ordering.(*39*)
- $\tilde{T}$ is the ratio between two transition temperatures of the pure LC molecules (see Equation (43)).
- $\tilde{\nu}$ is the constant related to the nematic interaction (see Equation (45)).
- $\tilde{c}$ is the constant related to the chiral interaction (see Equation (47)).
- γ_i is the DP coupling of the LC molecule i.

In the following, we set $n_A = 4$ ($\chi_A = 127°$), $n_B = 3.5$ ($\chi_B = 120°$), and $Q_A = Q_B = 0.1$. We show the effects of the DP coupling γ_i on the phase diagrams. In this paper, we focus on binary mixtures with a good solubility and then we take the interaction parameter $\chi_{FH} = 0$ in Equation (3). When $\chi_{FH} = 0$, the isotropic interaction between LC molecules A and B is zero and then there are no macroscopic phase separations in the mixture. However when χ_{FH} is non zero, the critical point of the phase separations is given by $\chi^c_{FH} = (\sqrt{n_A}+\sqrt{n_B})^2/2n_An_B$.(*45*) When $\chi_{FH} > \chi^c_{FH}$, the phase separation takes place in the mixtures. It will be important in LC polymer and LC mixtures.(*46*)

Figure 4 shows the phase diagrams on the temperature $\tau_A(= T/T_{NI,A})$ and concentration (ϕ_B) plane with $\gamma_A = 0.003$ for various values of γ_B: $\gamma_B = 0$ (a), $\gamma_B = 0.0001$ (b), $\gamma_B = 0.001$ (c), $\gamma_B = 0.003$ (d), $\gamma_B = 0.005$ (e), and $\gamma_B = 0.016$

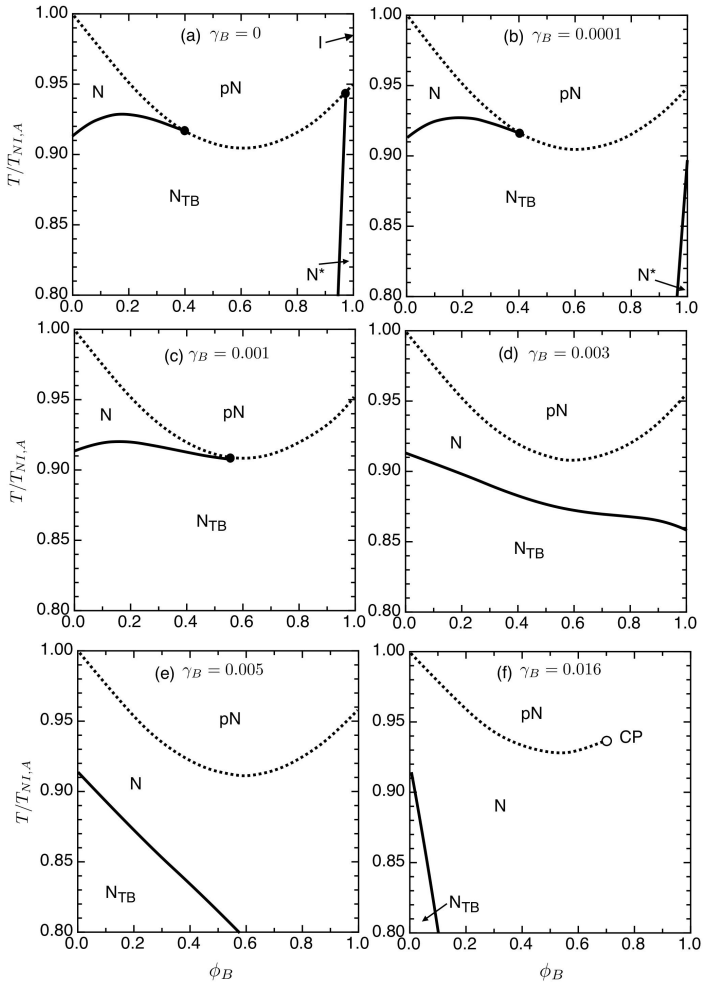

Figure 4. Phase diagrams on the temperature ($T/T_{NI,A}$) and concentration (ϕ_B) plane with $\tilde{T} = 0.95$, $\tilde{\nu} = 0.85$, $\tilde{c} = 1.05$, and $\gamma_A = 0.003$ for various values of γ_B: $\gamma_B = 0$ (a), $\gamma_B = 0.0001$ (b), $\gamma_B = 0.001$ (c), $\gamma_B = 0.003$ (d), $\gamma_B = 0.005$ (e), and $\gamma_B = 0.016$ (f). The solid curves show the second-order phase transitions: $N - N_{TB}$ and $N_{TB} - N^*$ transitions. The dotted-curves show the first-order phase transitions: $pN - N$, $pN - N_{TB}$, and $pN(I) - N^*$ transitions. Closed circles show the tricritical points (TCPs), at which the second-order phase transition line meets the first-order one and three phases coexist.

(f). We here define $\tilde{T}(\equiv T_{N^*I,B}/T_{NI,A}) = 0.95$, $\tilde{\nu} = 0.85$, and $\tilde{c} = 1.05$. From Equation (44), we then obtain $\epsilon_n = 0.88$, $\epsilon_{nB} = 1.086$, $\epsilon_x = 1.1$, and $\epsilon_{xB} = 1.086$. The reduced-temperature $T/T_{NI,A}$ is normalized by the $N - pN$ transition temperature of the pure molecule A at $\gamma_A = 0.003$ (see Figure 3 (a)). The $N - N_{TB}$ transition of the pure molecule A occurs at $T/T_{NI,A} = 0.913$ for $\gamma_A = 0.003$. The solid curves show the second-order phase transitions: $N - N_{TB}$ and $N_{TB} - N^*$ transitions. The dotted-curves show the first-order phase transitions: $pN - N$, $pN - N_{TB}$, and $I(pN) - N^*$ transitions. The closed circles show the tricritical points (TCPs), at which the second-order phase transition line meets the first-order one. Figure 4(a) shows the phase diagram for $\gamma_B = 0$. In this case, the director-pitch coupling of the molecule B is zero and then the $I - N^*$ phase transition only takes place, as shown in Figure 3(a), for the pure molecule B ($\phi_B = 1$) at $\tilde{T} = 0.95$. The $pN - N$ phase transition curve has a minimum as a function of ϕ_B because of $\tilde{\nu} = 0.85(< 1)$: the nematic interaction between dissimilar molecules is weak relative to that in the same species. The $N - N_{TB}$ transition curve has a maximum as a function of ϕ_B at the dilute region because of $\tilde{c} = 1.05(> 1)$: the chiral interaction between dissimilar molecules is strong relative to that in the same species. The $pN - N$ transition curve meets the $N - N_{TB}$ transition curve at the TCP. We also

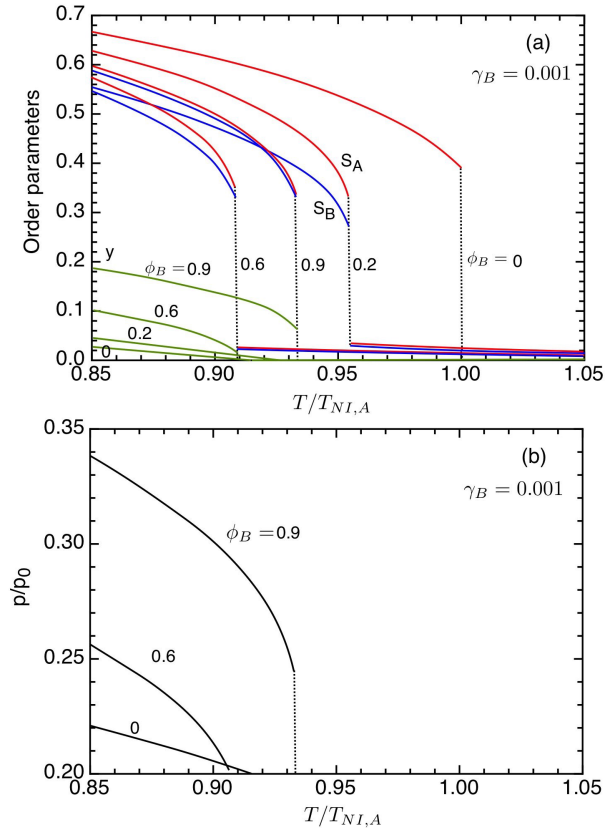

Figure 5. (color online) (a) Order parameters S_A, S_B, and y plotted against the temperature for various values of ϕ_B=0, 0.2, 0.6, 0.9 with $\gamma_B = 0.001$ in Figure 4(c). (b) pitch length p/p_0 plotted against the temperature for various values of ϕ_B=0, 0.6, 0.9 with $\gamma_B = 0.001$ in Figure 4(c).

find that the $pN - N_{TB}$ and the $N_{TB} - N^*$ transition curves cross at the another TCP, where pN, N_{TB}, and N^* phases coexist. The first-order $pN - N_{TB}$ phase transition appears and the stable N_{TB} phase appears in the broad range on the phase diagram. Figure 4(b) shows the phase diagram for $\gamma_B = 0.0001$. For the pure LC molecule B ($\phi_B = 1$), we have the first-order $pN - N_{TB}$ transition at $\tau_A = 0.95$ and the second-order $N_{TB} - N^*$ phase transition at $\tau_A = 0.895$. At $\tau_A \simeq 0.9$, the N_{TB} phase appears over all concentration ranges. As increasing the value of γ_B, the $N_{TB} - N^*$ transition temperature decreases and the TCP of the $N - N_{TB}$ phase transition shifts to higher concentrations (Figure 4(c)). When $\gamma_B = 0.003$, we have the $pN - N$ and $N - N_{TB}$ phase transitions at $\phi_B = 1$. The N phase appears between the pN and N_{TB} phases and the TCP disappears (Figure 4(d) and (e)). The similar phase diagrams have been experimentally observed.(*17, 19–21*) As shown in Figure 3(a), as increasing γ_B, the $pN - N$ transition temperature slightly shifts to higher temperatures and the $N - N_{TB}$ transition temperature shifts to lower temperatures. For the large γ_B, (Figure 4(f)), we find the critical point (CP, open circle) at the end of the $pN - N$ transition curve on the phase diagram. The N phase becomes dominant on the phase diagram because the director favors to align parallel to the pitch axis for a large γ_B.

Figure 5(a) shows the order parameters S_A, S_B, and y plotted against the temperature for various values of ϕ_B(=0, 0.2, 0.6, 0.9) with $\gamma_B = 0.001$ (Figure 4(c)). We have the first-order $pN - N$ transition, where the orientational order parameters jump as a function of temperature. The value of S_A is larger than that of S_B because of $n_A > n_B$ and $\tilde{T} < 1$. The orientational order parameters are nonzero in the high temperature region, which is the evidence of the pN phase that is not dis-

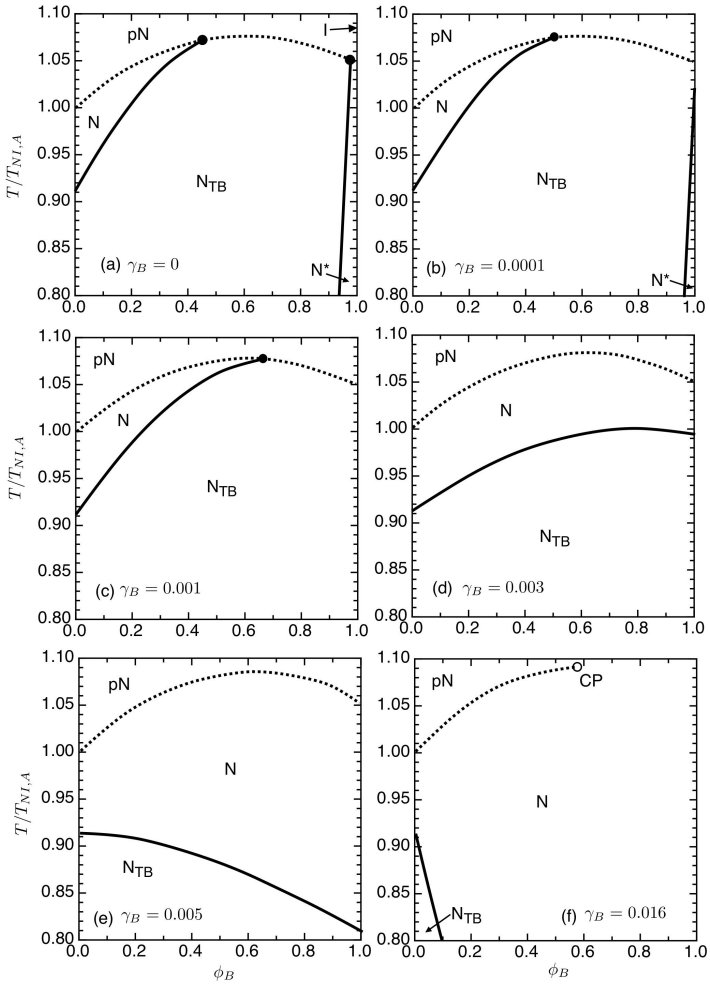

Figure 6. Phase diagrams on the temperature ($T/T_{NI,A}$) and concentration (ϕ_B) plane with $\tilde{T} = 1.05$, $\tilde{\nu} = 1.1$, $\tilde{c} = 1.05$, $Q_A = Q_B = 0.1$, and $\gamma_A = 0.003$ for various values of γ_B: $\gamma_B = 0$ (a), $\gamma_B = 0.0001$ (b), $\gamma_B = 0.001$ (c), $\gamma_B = 0.003$ (d), $\gamma_B = 0.005$ (e), and $\gamma_B = 0.016$ (f). The solid curves show the second-order phase transitions: $N - N_{TB}$ and $N_{TB} - N^*$ transitions. The dotted-curves show the first-order phase transitions: $pN - N$, $pN - N_{TB}$, and $pN(I) - N^*$ transitions. Closed circles show the tricritical points (TCPs), at which the second-order phase transition line meets the first-order one and three phases coexist.

ordered isotropic phase, while the values of S_i are very small values. Then the pN phase corresponds to the I phase observed experimentally.(*17*) When $\phi_B = 0.2$, the second-order $N - N_{TB}$ transition occurs at $\tau_A = 0.923$, where the order parameter y of the N_{TB} phase continuously increases from zero with decreasing temperature. When $\phi_B = 0.6$ and 0.9, we have the first-order $pN - N_{TB}$ phase transition, where the order parameter S_i and y jump at the transition temperature. Figure 5(b) shows the pitch length p/p_0 plotted against the temperature for various values of ϕ_B=0, 0.6, 0.9 with $\gamma_B = 0.001$ in Figure 4(c). When $\phi_B = 0$, the wavenumber at the $N - N_{TB}$ phase transition temperature is given by $Q^*_{TN}/Q_A = (K_2/K_3) = 5$ (see below Equation (40)) and the pitch p/p_0 continuously increases from $0.2(=K_3/K_2)$. When $\phi_B = 0.6$ and 0.9, the pitch p/p_0 discontinuously jumps at the $pN - N_{TB}$ transition and increases with decreasing temperature.

Figure 6 shows the phase diagrams on the temperature $\tau_A(= T/T_{NI,A})$ and concentration (ϕ_B) plane with $\gamma_A = 0.003$ for various values of γ_B: $\gamma_B = 0$ (a), $\gamma_B = 0.0001$ (b), $\gamma_B = 0.001$ (c), $\gamma_B = 0.003$ (d), $\gamma_B = 0.005$ (e), and $\gamma_B = 0.016$ (f). We here set $\tilde{T}(= T_{N^*I,B}/T_{NI,A}) = 1.05$, $\tilde{\nu} = 1.1$, and $\tilde{c} = 1.05$. From Equation (44), we obtain $\epsilon_n = 1.2$, $\epsilon_{nB} = 1.2$, $\epsilon_x = 1.15$, and $\epsilon_{xB} = 1.2$. When $\tilde{\nu} > 1$, the $pN - N$ transition curve has a maximum as a function of ϕ_B. The $N - N_{TB}$ transition

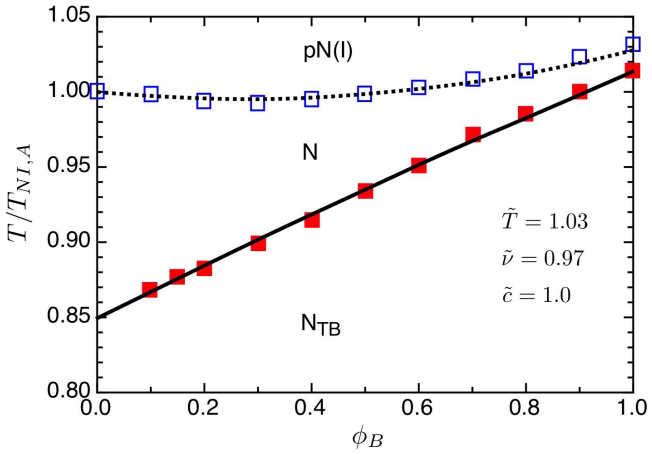

Figure 7. (color online) Comparisons between the theory and the experimental phase diagram for the binary mixtures of two LC molecules KA (molecule A) and CBF9CBF (molecule B): the open squares denote the $N-I$ transition and the closed squares denote the $N-N_{TB}$ transition.(*17*) The theoretical solid curve shows the second-order $N-N_{TB}$ transition and the dotted-curves show the first-order $N-pN$ transition with $\gamma_A = 0.0036$ and $\gamma_B = 0.002$.

temperature increases with increasing ϕ_B because of $\tilde{c} = 1.05(> 1)$ in Figures 6(a)-(d). As increasing γ_B, the TCP shifts to higher concentrations and the $N - N_{TB}$ transition appears for the pure LC molecule B. In Figure 6(d), the N phase appears between the pN and N_{TB} phases for all concentrations. Further increasing γ_B, the $N - N_{TB}$ transition temperature of the binary mixture decreases with increasing ϕ_B (Figure 6(e)). In Figure 6(f), the N phase becomes dominant on the phase diagram and the CP appears at the end of the $pN - N$ transition.

Our theory predicts various phase diagrams depending on the strength of the DP coupling γ_i of the LC molecule i. Some phase diagrams have been observed experimentally. In the next subsection, we compare our theory with the experimental phase diagrams.

3.4. *Comparisons of theory and experimental phase diagram*

In this subsection, we compare our theory with experimental phase diagrams for binary mixtures of banana-shaped LC molecules. In the followings, we set $Q_A = Q_B = 0.1$.

Figure 7 shows the comparison between our theory (solid and dotted curves) and the experimental phase diagram for the binary mixtures of two LC molecules KA (molecule A) and CBF9CBF (molecule B): the open squares denote the $I - N$ transition and the closed squares show the $N - N_{TB}$ transition.(*17*) The experimental phase diagram is similar to Figure 4(d) and 6(d), where the N phase appears between $pN(I)$ and N_{TB} phases for all concentrations. The theoretical solid curve shows the second-order $N-N_{TB}$ transition and the dotted-curve shows the first-order $pN - N$ transition. We here use $n_A = n_B = 4$ for the molecular parameters. The $I - N$ and $N - N_{TB}$ transition temperatures of the pure molecule A are $T_{NI,A} = 348$ K and $T_{N_{TB}N,A} = 295$ K, respectively. We then obtain $T_{N_{TB}N,A}/T_{NI,A} \simeq 0.848$, which corresponds to the ratio of the two transition temperatures at $\gamma_A = 0.0036$ in Figure 3(a). The $I - N$ and $N - N_{TB}$ transition temperatures of the pure molecule B are $T_{NI,B} = 359$ K and $T_{N_{TB}N,B} = 353$ K, respectively, and we set $\gamma_B = 0.002$ to be the best fitting. We also obtain the numerical parameter $\tilde{T} = T_{NI,B}/T_{NI,A} = 1.031$. The other numerical parameters set $\tilde{\nu} = 0.97$ and $\tilde{c} = 1.0$. The theory can quantitatively describe the experimental

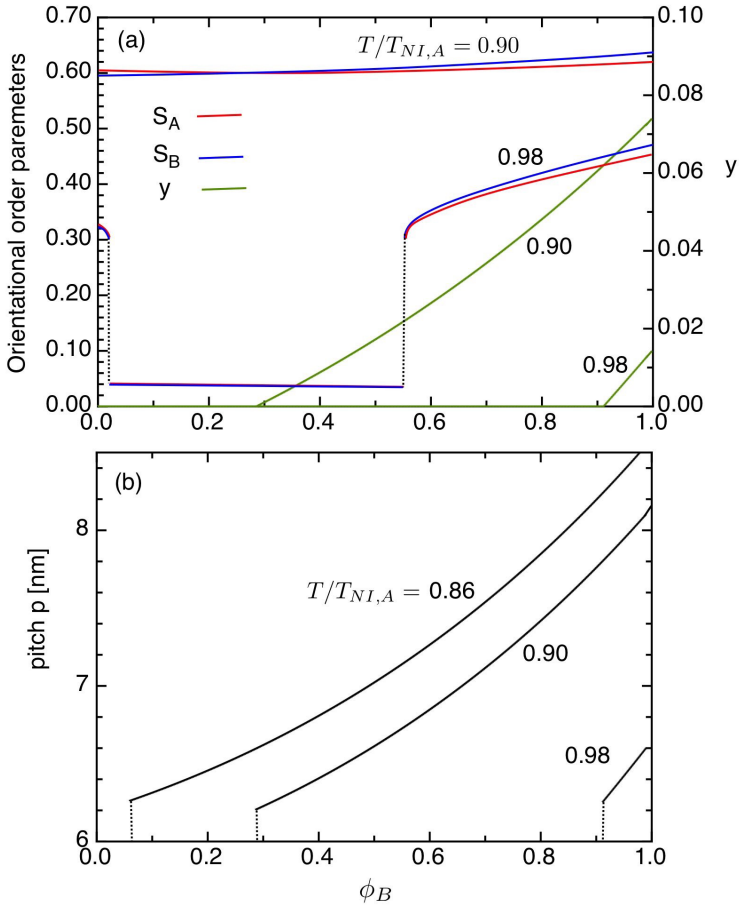

Figure 8. (color online) Order parameters (a) and pitch length p (b) as a function of ϕ_B for various temperatures in Figure 7. The pitch length is calculated by $p = 2\pi d_0/Q$ with $d_0 = 0.5$ nm.

phase diagram. The $N - pN(I)$ transition curve exhibits a slight concave curvature because of $\tilde{\nu} < 1$ and the $N - N_{TB}$ transition curve linearly increases with increasing ϕ_B because of $\tilde{c} = 1.0$. The N_{TB} phase is enhanced by adding the LC dimer CBF9CBF and the N phase appears between the narrow temperature range at $\phi_B = 1$. As shown in Figure 3(a), the N phase between the pN and N_{TB} phases can be controlled by the strength of the director-pitch coupling γ_i. As decreasing γ_i, the two transition temperatures $T_{N_{TB}N,i}$ and $T_{NI,i}$ approach and the N_{TB} phase appears at higher temperatures. In this mixture, we have $\gamma_A(= 0.0036) > \gamma_B(= 0.002)$ and the DP coupling of the KA (molecule A) is larger than that of the CBF9CBF (molecule B).

Using the same numerical parameters, we calculate the pitch length of the NT B phase on Figure 7. Figure 8 shows the order parameters (a) and pitch length p (b) as a function of ϕ_B for various temperatures in Figure 7. The pitch length of the N_{TB} phase is calculated by $p = 2\pi d_0/Q$ with $d_0 = 0.5$ nm. When $T/T_{NI,A} = 0.9$, the N_{TB} phase appears above $\phi_B > 0.29$ and the orientational order parameters (a) are almost constant $S_i \simeq 0.6$ and the pith length (b) increases with ϕ_B. When $T/T_{NI,A} = 0.98$, the pN phase with a small orientational order $S_i \simeq 0.04$ appears between two N phases and then the experimental I phase corresponds to the pN phase in our model.

Figure 9 shows the comparison of our theory (solid and dotted curves) with the experimental phase diagram for the binary mixtures of two LC molecules CB9CB (molecule A) and cpd8 (molecule B): the open squares denote the $N-I$ transition, the closed squares denote the $N - N_{TB}$.(*19*) The theoretical solid curve shows the

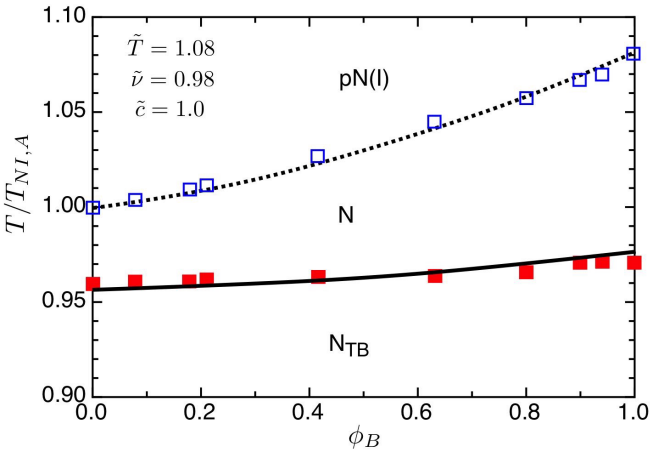

Figure 9. (color online) Comparisons between the theory and the experimental phase diagram for the binary mixtures of two LC molecules CB9CB (molecule A) and cpd8 (molecule B): the open squares denote the $N-pN(I)$ transition and the closed squares denote the $N-N_{TB}$ transition.(*19*) The theoretical solid curve shows the second-order $N-N_{TB}$ transition and the dotted-curves show the first-order $pN(I)-N$ transition with $\gamma_A = 0.0034$ and $\gamma_B = 0.003$.

second-order $N-N_{TB}$ transition and the dotted-curve shows the first-order $pN-N$ transition. We use $n_A = 2.9$ ($\chi_A = 110°$) and $n_B = 4.1$ ($\chi_B = 128°$) due to the experimental bend angles. The $N-I$ and $N_{TB}-N$ transition temperatures of the CB9CB (molecule A) are $T_{NI,A} = 394.5$ K and $T_{N_{TB}N,A} = 378.4$ K, respectively. We then obtain $T_{N_{TB}N,A}/T_{NI,A} \simeq 0.959$ and use $\gamma_A = 0.0034$. The $N-I$ and $N_{TB}-N$ transition temperatures of the cpd8 (molecule B) are $T_{NI,B} = 426.3$ K and $T_{N_{TB}N,B} = 382.9$ K, respectively, and we set $\gamma_B = 0.003$ for the coupling parameters to be the best fitting. We also obtain the numerical parameter $\tilde{T} = T_{NI,B}/T_{NI,A} = 1.08$. The other numerical parameters set $\tilde{\nu} = 0.98$ and $\tilde{c} = 1.0$. The theory can quantitatively describe the experimental phase diagram. The $N-pN(I)$ transition curve exhibits a slight concave curvature because of $\tilde{\nu} = 0.98$ and the $N-N_{TB}$ transition curve linearly increases with increasing ϕ_B because of $\tilde{c} = 1.0$. In this mixture, we have $T_{N_{TB}N,A} \simeq T_{N_{TB}N,B}$ and the strength of the DP coupling has almost the same value: $\gamma_A(= 0.0036) \simeq \gamma_B(= 0.003)$

Figure 10 shows the order parameters (a) and the pitch length p (b) as a function of ϕ_B at $T/T_{NI,A} = 0.9, 0.92, 0.94$ in Figure 8. The pitch length is calculated by $p = 2\pi d_0/Q$ with $d_0 = 0.5$ nm. The order parameters (Figure 10(a)) are almost constants as a function of ϕ_B. As decreasing temperature at a given ϕ_B, the order parameters and the pitch length increase. In the N_{TB} phase, the orientational order parameter S_B is slightly larger than S_A, because of $n_B > n_A$ and $\tilde{T} > 1$. The order parameter y has small values. For example, when $y = 0.02$, we have the cone angle $\epsilon = 10°$. The pitch length (Figure 10(b)) has a minimum value as a function of ϕ_B. Using Equation (35), the pitch length of the N_{TB} phase is approximately given by

$$\frac{p}{p_A^\circ} \simeq \sqrt{\frac{1-2(1-\epsilon_n)\phi_B + (1-2\epsilon_n+\epsilon_{nB})\phi_B^2}{1+\left(\frac{\gamma_B}{\gamma_A}-1\right)\phi_B}}, \tag{51}$$

where we have assumed $S_A \simeq S_B$ and $p_A^\circ \equiv d_0(\tilde{k}_3\nu_A S_A/6\gamma_A)^{1/2}$ is the pitch length of the pure LC molecule A. From Equation (46), we have $\epsilon_n = 0.856$ and $\epsilon_{nB} = 0.764$. Then the pitch length has a concave curvature as a function of ϕ_B. For larger values of $\epsilon_n(> 1)$, for example, in Figure 6(d), the pitch length has a convex curvature as a function of ϕ_B. It has been observed that the pitch of the N_{TB} phase is about $p = 8$ nm in the bent molecular dimers CB7CB.(*7*) The orientational order

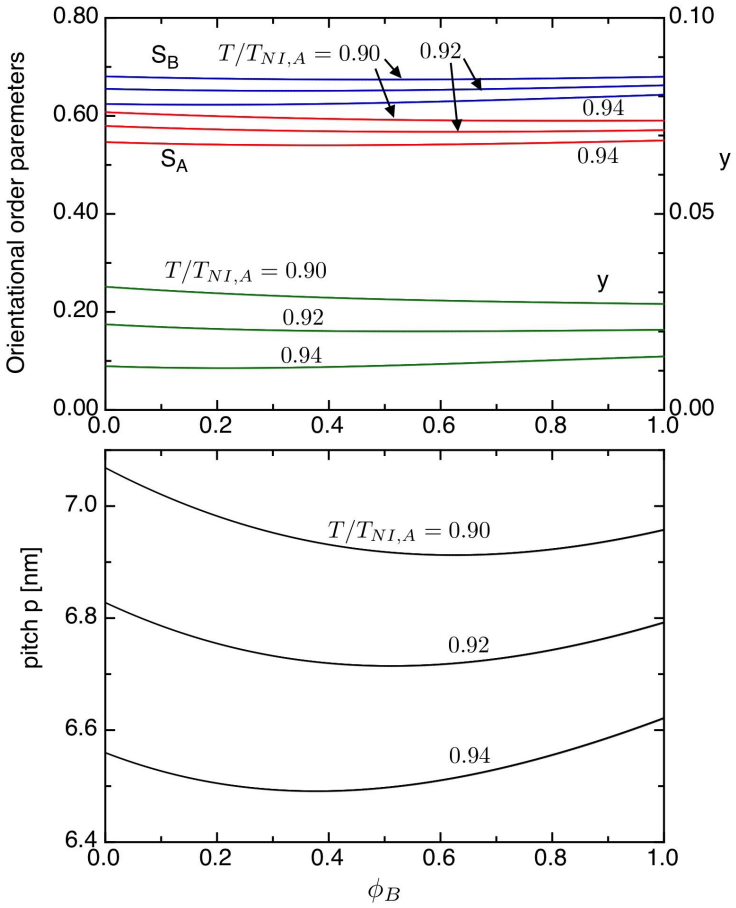

Figure 10. (color online) Order parameters (a) and pitch length p (b) of the N_{TB} phase as a function of ϕ_B at $T/T_{NI,A} = 0.9, 0.92, 0.94$ in Figure 9. The pitch length is calculated by $p = 2\pi d_0/Q$ with $d_0 = 0.5$ nm.

parameter increases from 0.41 to 0.73 with decreasing temperature in a mixture of CB7CB and LC molecule KA.(*17*) Our numerical calculations are the same order with the experimental data.

Figure 11 shows the comparison of our theory (solid and dotted curves) with the experimental phase diagram for the binary mixture of two LC dimers 2O.5.O2 (molecule A) and 2O.3.O2 (molecule B): the open squares denote the $N-I$ transition, the closed squares denote the $N-N_{TB}$, and the open circles show the $N_{TB}-I$ transition.(*20*) The LC dimers 2O.5.2O and 2O.3.2O have odd spacers 5 and 3, respectively. We here set $n_A = 4$ ($\chi_A = 127°$) and $n_B = 3.7$ ($\chi_B = 123°$). The experiment shows that the N_{TB} phase is formed directly from the I phase via a strong first-order phase transition,(*20*) which is demonstrated in Figure 5(a). The pure LC molecule B has the $N_{TB}-I$ transitions and then the experimental $N_{TB}-I$ transitions correspond to the phase diagrams with the weak DP coupling γ_B as shown in Figure 4(b)-(c). We here use $\gamma_B = 0.001$ as shown in Figure 4(c) for the numerical calculation. The $N-I$ transition and the $N_{TB}-N$ transition temperature of the 2O.5.2O molecule (A) are $T_{NI,A} = 385.3$ K and $T_{N_{TB}N,A} = 366.9$ K, respectively. We then obtain $T_{N_{TB}N,A}/T_{NI,A} \simeq 0.952$ and can estimate $\gamma_A = 0.00255$ from Figure 3(a) for the best fitting. The $N_{TB}-I$ transition temperature of the 2O.3.2O molecule (B) is $T_{N_{TB}I,B} = 360.4$ K and we then obtain the numerical parameter $\tilde{T} = T_{N_{TB}I,B}/T_{NI,A} = 0.9353$. We also set $\tilde{\nu} = 0.95$ and then we have $\epsilon_n = 0.96$, $\epsilon_x = 0.99$, and $\epsilon_{nB} = 1.011$. The chiral parameter is changed: $\tilde{c} = 0.95$, 1.0 and 1.1. The $pN(I)-N$ transition curve has

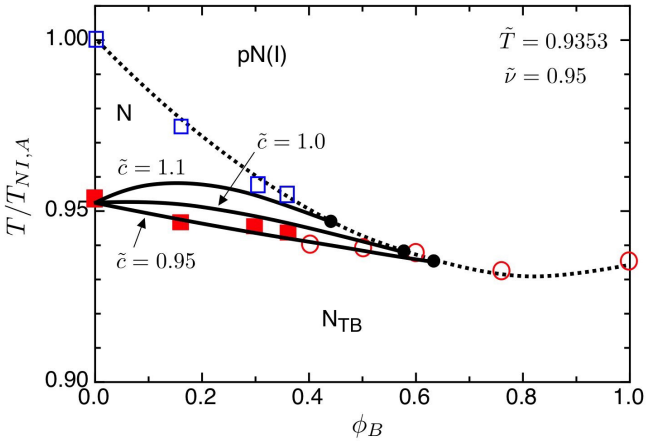

Figure 11. (color online) Comparisons between the experimental phase diagram and theory. The symbols show the experimental phase diagram for the binary mixtures of two LC dimers 2O.5.O2 (molecule A) and 2O.3.O2 (molecule B): the open squares denote the $N-I$ transition, the closed squares denote the $N-N_{TB}$, and the open circles show the $N_{TB}-I$ transition.(*20*) The theoretical solid curves show the second-order $N-N_{TB}$ transition and the dotted-curve shows the first-order phase transitions: $pN(I)-N$ and $pN(I)-N_{TB}$ transitions. The chiral parameter is changed: $\tilde{c}=0.95$, 1.0 and 1.1, with $\gamma_A=0.00255$ and $\gamma_B=0.001$.

a concave curvature as a function of ϕ_B because of $\tilde{\nu}<1$. The $N-N_{TB}$ transition for $\tilde{c}>1$ ($\tilde{c}<1$) has a convex (concave) curvature as a function of ϕ_B. The theory indicates that the TCP (closed circle) shifts to lower concentrations of ϕ_B with increasing the chiral parameter $\tilde{c}$. The theory can qualitatively describe the experimental phase diagram. The $pN(I)-N_{TB}$ phase transition is the first-order phase transition, where the orientational order parameter S_i jumps and strongly depends on the nematic interaction parameter $\tilde{\nu}$. Then the $pN(I)-N_{TB}$ phase transition curve does not depend on the chiral interaction parameter $\tilde{c}$. The chiral interaction parameter $\tilde{c}$ affects the second-order $N-N_{TB}$ phase transition. In this mixture, we have $\gamma_A(=0.00255)>\gamma_B(=0.001)$ and the DP coupling of the 2O.5.2O (molecule A) is larger than that of the 2O.3.2O (molecule B). As shown in Figure 3(a), the $pN(I)-N_{TB}$ transition exists between $\gamma_B^l<\gamma_B<\gamma_B^h$ and the $N-N_{TB}$ transition appears with $\gamma_A^h<\gamma_A$. The experimental phase diagram is similar with Figure 4(a)(b)(c), in which $\gamma_A>\gamma_B$.

Figure 12 shows the order parameters (a) and pitch length p (b) as a function of ϕ_B at $T/T_{NI,A}=0.9, 0.92, 0.94$ with $\tilde{c}=1$ in Figure 10. The pitch length is calculated by $p=2\pi d_0/Q$ with $d_0=0.5$ nm. As decreasing temperature at a given ϕ_B, the order parameters and the pitch length increase. When $T/T_{NI,A}=0.9$ and 0.92, the mixture is in the N_{TB} phase, where the value of the order parameter y and the pitch length (p) increase with increasing ϕ_B. When $T/T_{NI,A}=0.94$, we have the second-order $N_{TB}-N$ phase transition at $\phi_B=0.52$, at which the value of y continuously changes with decreasing ϕ_B and the first-order $N-pN(I)$ transition takes place at $\phi_B=0.56$, at which the orientational order parameters jump (Figure 12(a)). Due to the experimental observations of the quadrupolar splittings for the 2O.7.2O molecule, the order parameter grows from about 0.27 at T_{NI} to about 0.51 before the transition to the N_{TB} and has grown to 0.56 at the N_{TB} phase with decreasing temperature.(*3, 24*)

We demonstrate that the DP coupling γ_i of the LC molecule becomes an important parameter to understand the phase behaviors including the N_{TB} phase. Our theory predicts that there are various phase diagrams, depending on the value of γ_i. It is worth to point out that the Figures 4(a)(b) and 5(a)(b), including the N^* phase, with the weak coupling γ_i have not been observed yet. These phase diagrams

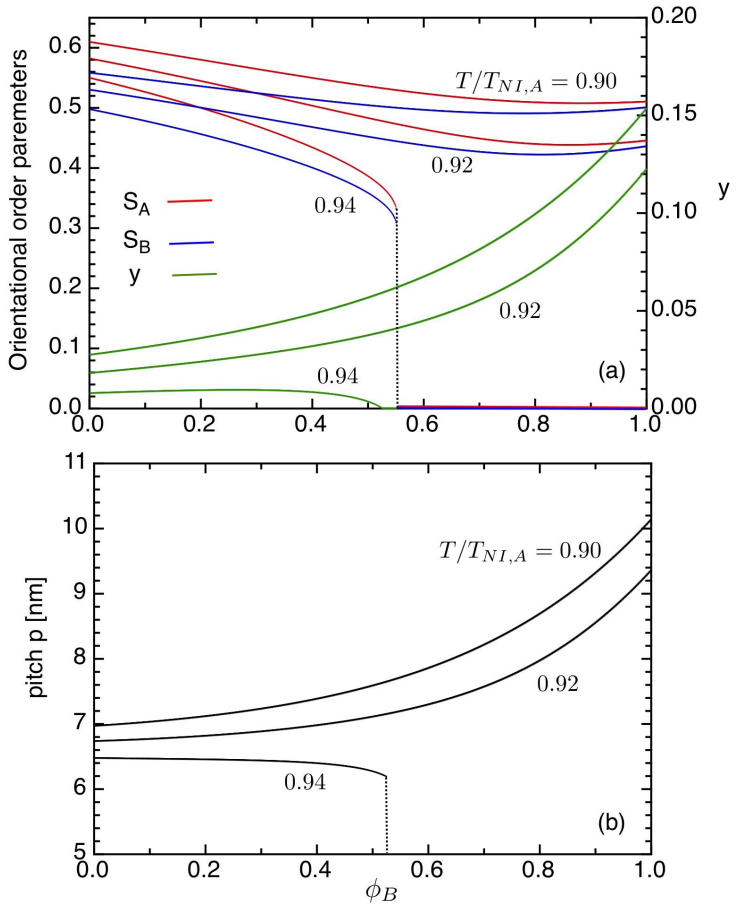

Figure 12. (color online) Order parameters (a) and pitch length p (b) as a function of ϕ_B at $T/T_{NI,A} = 0.9, 0.92, 0.94$ with $\tilde{c} = 1$ in Figure 10. As decreasing temperature at a given ϕ_B, the order parameters and the pitch length increase. The pitch length is calculated by $p = 2\pi d_0/Q$ with $d_0 = 0.5$ nm.

may be observed in the mixtures of a LC dimer such as CB7CB and a LC molecule with a $N^* - I$ transition. At the strong coupling γ_i, the CP appears as shown in Figures 4(f) and 5(f), which also have not been observed yet. The parameter γ_i corresponds to the local oblique twisting power and changes from N_{TB} to N phase, in which the director couples with the helical axis and affects the range of the N_{TB} phase. The experimental verification of the coupling parameter γ_i, or the local oblique twisting power, is open questions.

Our theory shows good agreements with the experimental phase diagrams. Most of the experimental phase diagrams observed so far has been fitted with $\gamma_i = 0.001 \sim 0.003$. These values correspond to the external electric field, applying parallel to the helix axis direction, approximately on the order of ~ 1 V/μm.(*39*) That means the strength of the director-pitch coupling corresponds to the local electric field on the order of $\sim$1 mV per a pitch length (order of nm) of the N_{TB} phase and it may give rise a local polarization. This becomes the local twisting power induced by the stacking parallel to the pitch axis of the banana-shaped LC molecules with a molecular dipole moment.(*22*) .

The flexoelectric effects may be important to the free energy of a N_{TB} phase. In a usual N phase, the director $\mathbf{n}$ is equivalent to $-\mathbf{n}$ and hence the electric polarization is zero. However a splay or a bending distortion can create an electric polarization $\mathbf{p}_f$ which is proportional to the first-order space derivatives of the director $\mathbf{n}$.(*55*) Due to the recent theoretical study based on the Frank elastic theory,(*38*) the flexoelectric polarization ($\mathbf{p}_f$) in the N_{TB} phases is perpendicular

to the nematic director (Equation (1)) and then the director-flexoelectric coupling is zero: $\mathbf{n}\cdot\mathbf{p}_f = 0$. Then the contribution to the free energy due to the flexoelectricity may be given by the coupling $-\mathbf{E}\cdot\mathbf{p}_f$, where $\mathbf{E}$ is an applied electric field. The coupling parameter γ_i between the director and helical axis is affected by the external magnetic or electric field applied parallel to the helical axis.(*28, 38*) Our theory can be extended to the N_{TB} phase including the flexoelectricity under the external fields.

4. Summary

We have demonstrated that our theory is capable of predicting a variety of phase diagrams for binary mixtures of banana-shaped LC molecules, in which the DP coupling $(-\gamma_i(\mathbf{n}\cdot\mathbf{p})^2)$ can be an important role for the spontaneous formation of the N_{TB} phase. The stable N_{TB} phase appears in the mixtures of $K_{22} > K_{33}$. The strength γ_i of the DP coupling for the LC molecule can affect the N_{TB} and phase diagrams. Physically, this parameter corresponds to a local oblique twisting power of the N_{TB} phase. For the weak coupling parameters, we have the first-order $pN(I) - N_{TB}$ transition with the TCP on the temperature-concentration plane (Figure 4(a)-(c) and 5(a)-(c)). Note that the pN phase has a very small orientational order and then it is realistically the I phase. Further increasing γ_i, the N_{TB} phase appears at lower temperatures of the N phase on the phase diagrams (Figure 4(d)(e) and 5(d)(e)). At the strong coupling γ_i, the N_{TB} phase disappears, or shifts to lower temperatures, and the first-order $pN(I) - N$ transition appears with the CP (Figure 4(f) and 5(f)). The parameters $\tilde{\nu}$ and $\tilde{c}$ relate the shape of the $pN(I) - N$ and $N - N_{TB}$ transition curves on the phase diagram, respectively. When $\tilde{c} > 1$ ($\tilde{c} < 1$), the $N - N_{TB}$ transition curve has a convex (concave) curvature as a function of the concentration.

Our theory has a good agreement with the experimental phase diagrams of the binary mixtures. The order parameters and pitch length of the N_{TB} phase are predicted as a function of the concentration for the experimentally observed phase diagrams. We have shown that most of the experimental phase diagrams can theoretically be reproduced with the values of $\gamma_i = 0.001 \sim 0.004$. These values correspond to the realistic values of the local oblique twisting power for the N_{TB} phase. Our theory can also be applicable to study phase separations in such binary mixtures.

References

(1) Meyer RB. Structural problems in liquid crystal physics, Les Houches Summer School in Theoretical Physics. In: Balian R, Weil G, editors. 1973 Molecular Fluids. New York (NY): Gordon and Breach: 1976. p. 273-373.

(2) Gortz V, Southern C, Roberts NW, Gleeson HF, Goodby JW. Unusual properties of a bent-core liquid-crystalline fluid. Soft Matter. 2009; 5: 463-471.

(3) Cestari M, Diez-Berart S, Dunmur DA, Ferrarini A, de la Fuente MR, Jackso, DJB, Lopez DO, Luckhurst GR, Perez-Jubindo MA, Ricardson RM, Salud J, Timimi BA, Zimmermann H. Phase behavior and properties of the liquid-crystal dimer 1", 7"-bis(4-cyanobiphenyl-4'-yl) heptane: A twist-bend nematic liquid crystal. Phys Rev E 2011: 84: 031704.

(4) Henderson PA, Imrie CT. Methylene-linked liquid crystal dimers and the twist-bend nematic phase. Liq Cryst. 2011; 38: 1407.

(5) Chen D, Porada JH, Hooper JB, Klittnick A, Shen Y, Tuchband MR, Korblova E, Bedrov D, Walba DM, Glaser MA, Maclennan JE, Clark NA. Chiral heliconical ground state of nanoscale pitch in a nematic liquid crystal of achiral molecular dimers. PNAS. 2013; 110: 15931-15936.

(6) Beguin L, Emsley JW, Lelli M, Lesage A, Luckhurst GR, Timimi BA, Zimmermann H. The Chirality of a Twist-Bend Nematic Phase Identified by NMR Spectroscopy. J Phys Chem B. 2012; 116: 7940-7951.

(7) Borshch V, Kim YK, Xiang J, Gao M, Jákli A, Panov VP, Vij JK, Imrie CT, Tamba MG, Mehl GH,

Lavrentovich OD. Nematic twist-bend phase with nanoscale modulation of molecular orientation. Nat Commun. 2013; 4: 2635.

(8) Sepelj M, Lesac A, Baumeister U, Diele S, Nguyen HL, Bruce DW. Intercalated liquid-crystalline phases formed by symmetric dimers with an α, ω-diiminoalkylene spacer. J Mater Chem 2007: 17: 1154-1165.

(9) Greco C, Luckhurst GR, Ferrarini A. Enantiotopic discrimination and director organization in the twist-bend nematic phase. Phys Chem Chem Phys. 2013; 15: 14961-14965.

(10) Meyer C, Luckhurst GR, Dozov I. Flexoelectrically Driven Electroclinic Effect in the Twist-Bend Nematic Phase of Achiral Molecules with Bent Shapes. Phys Rev Lett. 2013; 111: 067801.

(11) de Almeida RRR, Zhang C, Parri O, Sprunt SN, Jákli A. Nanostructure and dielectric properties of a twist-bend nematic liquid crystal mixture. Liq Cryst. 2014; 41: 1661-1667.

(12) Chen D, Nakata M, Shao R, Tuchband MR, Shuai M, Baumeister U, Weissflog W, Walba DM, Glaser MA, Maclennan JE, Clark NA. Twist-bend heliconical chiral nematic liquid crystal phase of an achiral rigid bent-core mesogen. Phys Rev E. 2014; 89: 022506.

(13) Challa PK, Borshch V, Parri O, Imrie CT, Sprunt SN, Gleeson JT, Lavrentovich OD, Jákli A. Twist-bend nematic liquid crystals in high magnetic fields. Phys Rev E. 2014; 89: 060501(R).

(14) Yun CJ, Vengatesan MR, Vij JK, Song JK. Hierarchical elasticity of bimesogenic liquid crystals with twist-bend nematic phase. Appl Phys Lett. 2015; 106: 173102.

(15) Hoffmann A, Vanakaras AG, Kohlmeier A, Mehl GH, Photinos DJ. On the structure of the Nx phase of symmetric dimers: inferences from NMR. Soft Matter. 2015; 11:850-855.

(16) Paterson DA, Gao M, Kim YK, Jamali A, Finley KL, et.al. Understanding the twist-bend nematic phase: the characterisation of 1-(4-cyanobiphenyl-4'-yloxy)-6-(4-cyanobiphenyl-4'-yl)hexane(CB6OCB) and comparison with CB7CB. Soft Matter. 2016; 12: 6827-6840.

(17) Adlem K, Copic M, Luckhurst GR, Mertelj A, Parri O, Richardson RM, Snow BD, Timimi BA, Tuffin RP, Wilkes D. Chemically induced twist-bend nematic liquid crystals, liquid crystal dimers, and negative elastic constants. Phys Rev E. 2013; 88: 022503.

(18) Mandle RJ, Davis EJ, Voll CCA, Archbold CT, Goodby JW, Cowling SJ. The relationship between molecular structure and the incidence of the N_{TB} phase. Liq Cryst. 2015; 42: 688-703.

(19) Mandle RJ, Archbold CT, Sarju JP, Andrews JL, Goodby JW. The dependency of nematic and twist-bend mesophase formation on bend angle. Sci Rep. 2016; 6: 36682.

(20) Dawood AA, Grossel MC, Luckhurst GR, Richardson RM, Timimi BA, Wells NJ, Yousif YZ. On the twist-bend nematic phase formed directory from the isotropic phase. Liq Cryst. 2015; 43: 2-12.

(21) Archbold CT, Davis EJ, Mandle RJ, Cowling SJ, Goodby JW. Chiral dopants and twist-bend nematic phase-induction of novel mesomorphic behaviour in an polar bimesogen. Soft Matter. 2015; 11: 7547-7557.

(22) Abberley JP, Jansze SM, Walker R, Patterson DA, Henderson PA, Marcelis ATM, Storey JMD, Imrie CT. Structure-property relationships in twist-bend nematogens: the influence of terminal groups. Liq Cryst. 2017; 44: 68-83.

(23) D 'Alessandro G, Luckhurst GR, Sluckin TJ. Twist-bend nematics and beyond, Liq Cryst. 2017; 44: 1-3.

(24) Dawood AA, Grossel MC, Luckhurst GR, Richardson RM, Timimi BA, Wells NJ, Yousif YZ, Twist-bend nematics, liquid crystal dimers, structure-property relations, Liq Cryst. 2017; 44: 106-126.

(25) Panov VP, Vij JK, Mehl GH, Twist-bend nematic in cyanobiphenyls and difluoroterphenyls, Liq Cryst. 2017; 44: 147-159.

(26) Xiang J, Shiyanovskii SV, Imrie C, Lavrentovich OD. Electrooptic Response of Chiral Nematic Liquid Crystals with Oblique Helicoidal Director. Phys Rev Lett. 2014; 112: 217801.

(27) Matsuyama A, Field-induced oblique helicoidal cholesteric phases in mixtures of chiral and achiral liquid crystalline molecules. Liq Cryst. 2017; DOI: 10.1080/02678292.2017.1323239.

(28) Matsuyama A, Theory of a helicoidal cholesteric phase induced by an external field. Liq Cryst. 2016; 43: 783-795.

(29) Thisayukta J, Nakayama Y, Watanabe J. Effect of chemical structure on the liquid crystallinity of banana-shaped molecule. Liq Cryst. 2000; 27: 1129-1135

(30) Thisayukta J, Niwano H, Takezoe H, Watanabe J. Enhancement of Twisting Power in the Chiral Nematic Phase by Introducing Achiral Banana-Shaped Molecules. J Am Chem Soc. 2002; 124: 3354-3358.

(31) Lubensky TC, Radzihovsky L. Theory of bent-core liquid-crystal phases and phase transitions. Phys Rev E. 2002; 66: 031704.

(32) Lansac Y, Maiti PK, Clark NA, Glaser M. A. Phase behavior of bent-core molecules. Phys Rev E. 2003; 67: 011703.

(33) Dozov I. On the spontaneous symmetry breaking in the mesophases of achiral banana-shaped molecules. Europhys Lett. 2001; 56: 247-253.

(34) Shamid SM, Dhakal S, Selinger JV. Statistical mechanics of bend flexoelectricity and the twist-bend phase in bent-core liquid crystals. Phys Rev E. 2013; 87: 052503.

(35) Shamid SM, Allender DW, Selinger JV. Predicting a Polar Analog of Chiral Blue Phases in Liquid Crystals. Phys Rev Lett. 2014; 113: 237801.

(36) Virga EG. Double-well elastic theory for twist-bend nematic phases. Phys Rev E. 2014; 89: 052502.

(37) Barbero G, Evangelista LR, Rosseto MP, Zola RS, Lelidis I. Elastic continuum theory: Towards understanding of the twist-bend nematic phases. Phys Rev E. 2015; 92: 030501(R).

(38) Zola RS, Barbero G, Lelidis I, Rosseto MP, Evangelista LR. A continuum description for cholesteric and nematic twist-bend phases based on symmetry considerations. Liq Cryst. 2017; 44: 24-30.

(39) Matsuyama A, Director-pitch coupling-induced twist-bend nematic phase. J Phys Soc Jpn. 2016; 85: 114606.

(40) Vanakaras AG, Photinos DJ. A molecular theory of nematic-nematic phase transitions in mesogenic dimers Soft Matter. 2016; 12: 2208-2220.

(41) Greco C, Luckhurst GR, Ferrarini A. Molecular geometry, twist-bend nematic phase and unconven-

tional elasticity: a generalised Maier-Saupe theory. Soft Matter. 2014; 10: 9318-9323.
(42) Ferrarini A. The twist-bend nematic phase: molecular insights from a generalised Maier-Saupe theory. Liq Cryst. 2017; 44: 45-57.
(43) Tomczyk W, Pajak G, Longa L. Twist-bend nematic phases of bent-shaped biaxial molecules. Soft Matter. 2016; 12: 7445-7452.
(44) Greco C, Ferrarini A. Entropy-driven chiral order in a system of achiral bent particles. Phys Rev Lett. 2015; 115: 147801.
(45) Flory PJ. Principles of polymer chemistry. Ithaca: Cornell University; 1953.
(46) Matsuyama A. Thermodynamics of flexible and rigid rod polymer blends. In: Isayev AI, editor. Encyclopedia of polymer blends. Vol. 1. Weinheim (Germany): WILEY-VCH; 2010. Chapter 2.
(47) Luckhurst GR, Gray GW. Ed. The Molecular Physics of Liquid Crystals. Academic Press, New York, 1979.
(48) Lin-Liu YR, Shih YM, Woo CW. Molecular theory of cholesteric liquid crystals and cholesteric mixtures. Phys. Rev. A **15**, 2550 (1977).
(49) Lin-Liu YR, Shih YM, Woo CW, Tan HT. Molecular model for cholesteric liquid crystals. Phys. Rev. A **14**, 445 (1976).
(50) Goossens WJA. A Molecular Theory of the Cholesteric Phase and of the Twisting Power of Optically Active Molecules in a Nematic Liquid Crystal. Mol Cryst Liq Cryst. 1971; 12: 237-244.
(51) Matsuyama A. Theory of polymer-dispersed cholesteric liquid crystals. J Chem Phys. 2013: 139; 174906.
(52) Matsuyama A. Biaxiality of cholesteric phases in rod-like polymer solutions. Liq Cryst. 2015; 42: 423-429.
(53) Maier W, Saupe A. Eine einfache molekular-statische theorie der nematischen kristallinflussigen phase. Teil I. Z Naturforsch. 1959; 14a: 882-889.
(54) Onsager L. The effects of shape on the interaction of colloidal particles. Ann NY Acad Sci. 1949; 51: 627-659.
(55) De Gennes PG, Prost J. The physics of liquid crystals. New York (NY): Oxford University Press; 1993
(56) Wojtowicz PJ, Sheng P. Critical point in the magnetic field-temperature phase diagram of nematic liquid crystals. Phys Lett A. 1974; 48: 235-236.
(57) Lelidis I, Durand G. Electric-field-induced isotropic-nematic phase transition. Phys Rev E. 1993; 48: 3822-3824.
(58) Sheng P. Boundary-layer phase transition in nematic liquid crystals. Phys Rev A. 1982;26: 1610-1617.
(59) Sheng P. Phase Transition in Surface-Aligned Nematic Films. Phys Rev Lett. 1976; 37: 1059-1062.
(60) Niori T, Sekine T, Watanabe J, Furukawa T, Takezoe H. Distinct ferroelectric smectic liquid crystals consisting of banana shaped achiral molecules. J Mater Chem. 1996; 6: 1231-1233.
(61) Chiu HW, Kyu T. Equilibrium phase behaviour of nematic mixtures. J Chem Phys. 1995; 103: 7471-7481.